Illegal Immigration and Infections: Evidence from Two Modern Pandemics

Lucas Shen *

December 2024

Abstract

The predominant attention on the global transmission of pandemics has centered on official travel. This study shifts the lens to the role of illegal immigration in the H1N1 and COVID-19 pandemics using trafficking inflow risk. The empirical strategy exploits cross-country differences in coastline lengths as a measure of porosity to instrument for trafficking risk, with fatality rates used as falsification tests. The findings show that countries with higher trafficking risk experience higher infection rates, but not higher fatality rates. Combining an augmented epidemiological model of transmission dynamics with high-frequency COVID-19 data, this study identifies early increases in contact rates as a key mechanism driving transmission. These results underscore the importance of early lockdowns in curbing transmission and expose possible gaps in public health systems for vulnerable populations during pandemics.

JEL Codes: F22; I12; I18; J61

Key words and phrases: Propagation of diseases, pandemics, illegal immigration, human trafficking, health economics, public health.

*The author gratefully thanks the editor, Sushanta Mallick, two anonymous referees, Paul Cheung, Ammu George, Giovanni Ko, Gaurav Sood, and Xie Taojun for comments and help on the paper. For brevity, both countries and territories are referred to as "countries." Maps delineating study areas do not necessarily depict accepted national boundaries.
Institute for Human Development and Potential, Agency for Science, Technology and Research. Email: lucas@lucasshen.com.

1 Introduction

Almost the entirety of the attention around stopping the initial international spread of pandemics has focused on "official" travel (e.g., St John et al. 2005; Ferguson et al. 2006; Khan et al. 2013; Khan and Singh 2014; Williams et al. 2015; Bogoch et al. 2016; Chinazzi et al. 2020; Fang et al. 2020; Kraemer et al. 2020; Shi et al. 2020; Rojanaworarit and El Bouzaidi 2021; Boto-García 2023; Stankov 2024). To that end, countries are swift to impose travel restrictions. Despite these measures, the H1N1 and COVID-19 quickly spread globally (Chinazzi et al. 2020). One reason these policies have fallen short is their lack of strictness—countries like New Zealand adopted stricter measures and successfully curbed the spread. But another part of the answer may lie in illegal migration (Kiss and Zimmerman 2019; Rojanaworarit and El Bouzaidi 2021, 2022).

Illegal immigrants, often residing in overcrowded conditions with limited access to healthcare, experience much higher transmission rates (Worsnop 2019; Chinazzi et al. 2020; Bojorquez et al. 2021; Rojanaworarit and El Bouzaidi 2021; Todres and Diaz 2021; Rojanaworarit and El Bouzaidi 2022). Consequently, illegal immigration may be an important vector of infections during a pandemic. If true, public health officials may need to tailor targeted policies geared toward illegal immigrants (Li et al., 2020).

Using data from the two recent pandemics, I evaluate whether illegal immigration, including human trafficking, is a hidden vector of infectious disease transmission.[1] To identify the effect of trafficking on the number of cases in the H1N1 and COVID-19 pandemic episodes, I link human trafficking inflow risk (Frank 2013) to the number of cases per population. Controlling for proximity to source countries and holding regional factors constant, the ordinary least squares (OLS) estimates suggest that countries with higher trafficking risk have more cases per population. Going from the 25th to the 60th percentile in the trafficking risk measure increases case numbers by approximately 1.35 times.

Since trafficking flows are unlikely to be exogenous, I use the coastline length to land

[1] While illegal immigrants and trafficked persons fall under distinct legal and humanitarian frameworks, their pathways into illegal border crossings often overlap through organized migrant smuggling (U.S. Department of State 2001), with similar public health implications due to adverse living and working conditions (Kiss and Zimmerman 2019; Bojorquez et al. 2021; Rojanaworarit and El Bouzaidi 2021; Todres and Diaz 2021; Rojanaworarit and El Bouzaidi 2022). Additionally, both groups contribute to the pool of untraceable cases, acting as significant vectors for transmission (Li et al. 2020; Page et al. 2020; Rojanaworarit and El Bouzaidi 2021, 2022).

area ratio as an instrument for trafficking. I assume that longer coastlines are more porous (with increasing monitoring costs) and thus lead to a higher risk of trafficking inflows. Section 2.4 establishes the increasing appreciation of coastlines and maritime trafficking by sea as key channels for illegal entries because of the difficulty of monitoring sea borders and coastlines (UNODC [United Nations Office on Drugs and Crimes] 2016, p. 104). Italy, for instance, "received 23,370 irregular arrivals by sea" in 2018 alone (U.S. Department of State 2019, p. 259).

The coastline instrument technically only affects the probability of success. It does not entirely explain the demand for migration. The key endogeneity concern is that regions attracting trafficking inflow have better economic opportunities (Bales 2007; Cho 2015). Such regions are better connected and urbanized, potentially leading to higher transmissions. On the other hand, these regions typically also have better health outcomes with lower disease mortality. The above suggests that if trafficking risk is an exogenous instrument, it should predict infections but not disease mortality. This is precisely what I find when I use fatality rates as a placebo outcome measure in falsification tests.

To further test for robustness, I control for a wide range of cross-border movement factors, institutional and health factors, social-cultural factors, and geographical factors to weaken the assumptions (Section 5.1). The results are robust except when including the log health expenditure per capita control. A further caveat is that excluding (Northern and Western) European countries nearly doubles the standard errors, even though the estimates remain similar and statistically different from zero (Section 5). To further support the exclusion restriction (Section 5.2), I use data from drug inflows and seizures as alternative instruments, exploiting the connection between drug and human trafficking routes (UNODC [United Nations Office on Drugs and Crimes] 2011; Slack and Campbell 2016; UNODC [United Nations Office on Drugs and Crimes] 2018). While the robustness and placebo tests help rule out competing explanations, the results should be interpreted cautiously, particularly regarding causality.

A second set of analyses uses an augmented Susceptible-Infectious-Recovered-Deceased (SIRD) model to investigate contact rates as a mechanism explaining an increase in cases via trafficking (Section 6). Rojanaworarit and El Bouzaidi (2021) document how labor trafficking led to an outbreak of thousands of cases in a Thailand market. Many of these cases were asymptomatic and eventually spread to more than half the country through contact between illegal migrant workers and middlemen who operate across multiple markets. Such asymptomatic and undocumented cases are critical transmission vectors in the rapid spread of COVID-19 (Li et al., 2020; Page et al., 2020). To test such increases in contact rates as a specific channel, I model trafficking risk as increasing the contact rate in a SIRD model. With reasonable assumptions for tractability, I derive a model grounded in SIRD epidemiological foundations. I then exploit the availability of high-frequency data of case numbers and government responses for the COVID-19 pandemic to test whether and when trafficking risk increases transmission through the contact rate. The estimates suggest that countries with higher trafficking risks have higher increases in cases per population, but only in the earlier months (Feb–Mar). Once again, this pattern does not extend to fatality rates as a placebo outcome. Overall, the SIRD-based results suggest that early in the COVID-19 pandemic, going from the 25th to the 60th percentile in trafficking risk increases the contact rate by a factor of 0.43.

The study connects to a growing set of literature highlighting public health security around vulnerable undocumented migrants. Disease control measures typically emphasize biomedical principles, e.g., testing and safe distancing, for the general population (Rojanaworarit and El Bouzaidi 2021). However, social inequalities mean such measures do not travel to vulnerable subpopulations. Illegal migrants typically work in labor markets with high levels of public-facing contact (Rojanaworarit and El Bouzaidi 2021; Todres and Diaz 2021). Moreover, language barriers perpetuate health illiteracy and poorer compliance to basic preventive measures (Chinazzi et al. 2020; Rojanaworarit and El Bouzaidi 2021; Bojorquez et al. 2021; Rojanaworarit and El Bouzaidi 2022), and crowded living conditions limit self-isolation (Todres and Diaz 2021; Bojorquez et al. 2021).

Overall, the findings reinforce the need for safe-distancing measures and closures at critical points of pandemics to curb contact, as evidenced by how contact rates as a mechanism only play a role in earlier months. Once closures and lockdowns happen, the estimates suggest that trafficking no longer increases infectious contact. On the other hand, this same evidence of contact rates as a mechanism also exposes potential public health deficiencies in addressing social vulnerabilities that may exacerbate disease spread (Todres and Diaz 2021; Rojanaworarit and El Bouzaidi 2022).

The paper adds to the literature on how travel restrictions and mobility affect the spread of COVID-19 (Chinazzi et al. 2020; Fang et al. 2020; Kraemer et al. 2020; Kuchler et al. 2022; Li et al. 2020; Boto-García 2023), Zika virus (Bogoch et al. 2016), SARS (St John et al. 2005), H1N1 (Khan et al. 2013), and MERS (Williams et al. 2015). Outside of pandemics, human flows leading to disease spread are documented as early as Diamond (1997), noting how migration propagated the Spanish Flu from East Asia to the rest of the world in the early 20th century. More generally, this paper is related to studies connecting economic activity to the spread of viruses and diseases (Oster, 2012; Docquier et al., 2014; Adda, 2016; Djemai, 2018; Cunningham et al., 2020).

Section 2 outlines the main data and the instrumental variables strategy. Section 3 provides motivating facts and preliminary evidence. Section 4 reports the instrumental variables results. Section 5 reports an array of robustness tests. Section 6 tests the increase in contact rates as a plausible channel. Section 7 concludes.

2 Data and Empirical Strategy

2.1 Confirmed Cases and Deaths

The primary outcome variable is the number of confirmed cases per population in two recent pandemics: the H1N1 pandemic (also known as Influenza A or the swine flu) and the COVID-19 pandemic. H1N1 data comes from the World Health Organisation (WHO) and the European Centre for Disease Prevention and Control (ECDC), which includes confirmed cases and deaths in April–August 2009 (the pandemic subsided after that, and the ECDC reports became less frequent). COVID-19 numbers are from the Johns Hopkins University.[2]

Early observations have many missing records. This is most severe in the first month. Of the 301 country-pandemic episode observations (in the most inclusive baseline regres-

[2] Available at `https://github.com/CSSEGISandData/COVID-19`. Their data repository draws from numerous sources, including the WHO, ECDC, and other government organizations such as the CDCs (Centers for Disease Control) of China, Taiwan, and the US.

sions), 277 observations are missing in the first month (92.0%), 232 observations are missing by the second month (77.1%), and 76 observations are missing by the third month (25.2%). I assume zero cases for those observations not observed. The analyses in Section 3.3 and Section 4 focus on the 3rd month, as the first month with relatively complete data. These results are later replicated using data from other months for both pandemics (Section 4).

2.2 Human Trafficking Indicators

The data for the trafficking risk measure is the Human Trafficking Indicators dataset (Frank 2013). This resource compiles Trafficking in Persons (TIP) reports from the US Department of State's Office to Monitor and Combat Trafficking in Persons (TIP Office), which the office is obliged to collect under the *Victims of Trafficking and Violence Protection Act* of 2000 (Frank 2013). The dataset contains cross-country patterns in human trafficking and government efforts for 179 countries over 12 years (2000–2011). Please see Appendix A for how Frank (2013) constructs the indicators. The degree to which country c is a destination, as opposed to a source, in international trafficking is:

$$\text{Relative TIP inflow}_c = \frac{1}{T}\sum\nolimits_t \left(D_{ct} - S_{ct}\right) \tag{1}$$

where T = 12 for the twelve years in the data, D indicates the destination country, and S indicates the source country, with both on a scale of 0–3 (Fig. 1). For brevity, the Eq. (1) measure is also referred to as trafficking risk. While the indicators predate the COVID-19 pandemic by a few years, there is minimal variation over time. The median and modal year-to-year change in the above trafficking measure is zero (Fig. A1).

Fig. 1 plots the source vs. destination trafficking indicators to illustrate the trafficking measure. The measure in Eq. (1) is increasing in the risk of trafficking inflow and decreasing in the risk of trafficking outflow. The countries on the top left are those most at risk of trafficking outflow, e.g., Georgia (GEO) and Uruguay (URY). The countries on the bottom right are those most at risk of trafficking inflow, e.g., Italy (ITA) and Switzerland (CHE). Table A2 lists all countries and their trafficking inflow risk measure. The mean is -0.36, and the standard deviation is 2.15, with negative figures implying that the country is at

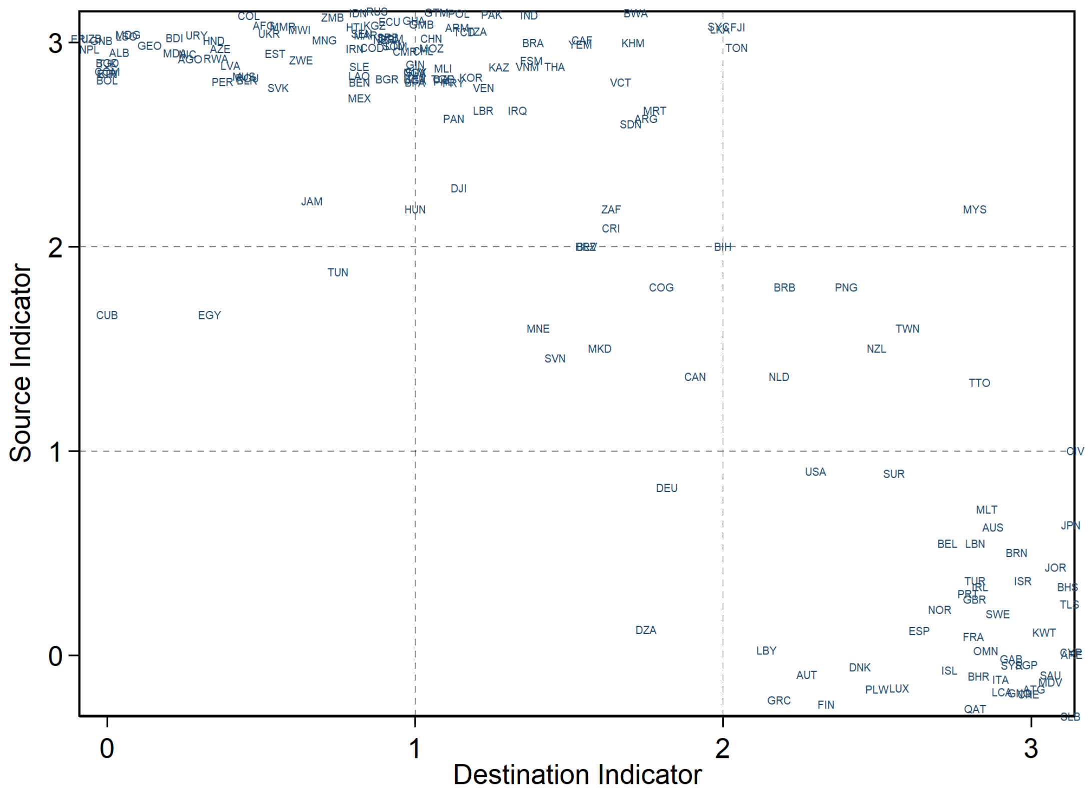

Fig. 1. Human trafficking risk indicators: Inflows (destination) versus outflows (source). Please see Table A2 for country codes and measures.

greater risk of facing trafficking outflow than inflow.[3]

2.3 Proximity and Bilateral Linkages

Data for gravity-type linkages include common language, common border, existing preferential trade agreement (PTA), and population-weighted distances (Gurevich and Herman 2018). Overall, these serve as controls for proximity to source countries. The "economics of language," for example, suggests that sharing a common primary language influences the destination of choice among immigrants (Chiswick and Miller 2015) as a supply-side factor, as shared languages reduce the cost of integration (e.g., finding work, accessing aid and services). On the other hand, the PTAs might include migration-related provisions affecting migration patterns as both demand- and supply-side factors (Beverelli and Orefice 2019).[4]

[3] Using only the mean of the destination indicator yields a value of 1.6 with a standard deviation of 0.98, which is lower than when other factors are included. The qualitative conclusions remain similar when relying solely on the destination indicator (Section 5.4).

[4] Section 5 considers additional bilateral controls as part of the international movement factors, including 5-year average estimates of bilateral international migration flows (Abel and Cohen 2019; see also Table A1).

2.4 Coastline Length to Land Area as an Instrument

The main subject of investigation in this paper is the cross-country link between human trafficking and the severity of the pandemic. The structural equation of interest is:

$$\text{(2)} \qquad \mathrm{y_{id}} = \delta_{\mathrm{d}} + \gamma_{\mathrm{i}} + \beta(\text{Relative TIP inflow})_{\mathrm{i}} + \mathbf{X}_{\mathrm{i}} + \mathbf{G}_{\mathrm{id}} + \varepsilon_{\mathrm{id}},$$

where $\mathrm{y_{id}}$ is the log of confirmed cases per million population for country i in pandemic episode d, and β captures the effect of trafficking on cases. The log transformation mitigates the influence of extreme values on the outcome measures. Additionally, it intuitively suggests that trafficking risk affects the stock of cases multiplicatively. This ties in with the mechanism where trafficking increases contact rates proportionally (discussed later in Section 6). δ_{d} is the dummy for the COVID-19 pandemic for epidemiological differences (with H1N1 pandemic the omitted category). γ_{i} includes 13 region dummies (Table A2). β is the main coefficient of interest, capturing the effect of the relative trafficking inflow risk measure (Eq. (1)) on the confirmed numbers per population. $\mathbf{X}_{\mathrm{i}}$ and $\mathbf{G}_{\mathrm{id}}$ are covariates for country characteristics and gravity-type proximity to source countries (Section 2.3). Source countries are omitted (Mexico for H1N1 and China for COVID-19).

Since a country's flows of trafficking and its pandemic severity are likely correlated with the quality of its institutions and economic connectivity, a direct cross-country comparison of the effect of trafficking risk and pandemic severity in Eq. (2) may be biased upwards. On the other hand, the opacity of true trafficking flows implies that the trafficking risk measure suffers from measurement error.[5]

To mitigate the endogeneity of the trafficking measure, I use the increasingly documented connection between international waters and human trafficking. The inaugural U.S. Department of State (2001) TIP report notes that the Hong Kong police force "continuously patrols land and sea boundaries to ensure border integrity and aggressively investigates triad involvement in organized migrant smuggling" (U.S. Department of State 2001 p. 20). In South Korea, much of their transit traffic occurs in their "territorial waters by

[5] For example, Italy and Switzerland had virtually the same trafficking measure in 2000–11 (3.9 and 4, respectively). However, the actual trafficking flows in these two countries likely differ to a greater extent than their trafficking measures suggest.

ship" (U.S. Department of State 2001, p. 97).

Coastlines and trafficking by sea are legitimate global concerns and key targets of international policy efforts. For instance, in Ireland's fishing industry, one of the recommendations is to "Amend the atypical working scheme for sea fishers to reduce their risk of labor trafficking" (U.S. Department of State 2019, p. 251). A TIP report recommends that Djibouti train its Coast Guard to better identify potential trafficking victims transiting by sea (U.S. Department of State 2019, p. 174). In Europe, Finland helped create an anti-trafficking curriculum for "trafficking victim identification for passenger ferry personnel in the Baltic Sea" (U.S. Department of State 2018, p. 188). Italian authorities conducted "joint border patrols and training with Slovenia and Albania, reportedly decreasing trafficking flows across the Adriatic Sea" (U.S. Department of State 2005, p. 131). The Swedish Coast Guard, police, and customs officials participated in similar "joint regional intelligence operations in trafficking cases involving travel by sea" (U.S. Department of State 2019, p. 440). Finally, in 2015, the United Kingdom passed the Modern Slavery Act, applicable to England and Wales, to "provide law enforcement authority to pursue criminals, including human traffickers at sea, and including authority to board, divert, and detain vessels; make arrests; and seize evidence while investigating potential offenses at sea" (U.S. Department of State 2019, p. 412).[6] [7]

Given this connection between coastlines and trafficking, in the first stage of the two-stage least-squares regression in Section 4, I instrument the trafficking risk measure (Eq. (1))

[6] Another potential channel through which coastline length can affect trafficking is the former's connection to the fishing industry, which is increasingly documented in the TIP reports. According to the UNODC [United Nations Office on Drugs and Crimes] (2016) report, trafficking for forced labor in the fishing industry "is commonplace in several parts of the world" (UNODC [United Nations Office on Drugs and Crimes] 2016, p. 8) and is "among the most frequently reported types of forced labor was trafficking in the fishing industry" (UNODC [United Nations Office on Drugs and Crimes] 2016, pp. 103–104). This type of fishing industry trafficking can happen "on board big fishing vessels on the high seas, carried out by large companies that trade fish internationally, or in on-land processing facilities" (UNODC [United Nations Office on Drugs and Crimes] 2016, p. 8). In Singapore, for example, a country with a legacy in seaports, fishing captains "engage in forced labor by using physical abuse to force men to perform labor on long-haul boats that transit or dock at Singaporean ports" (U.S. Department of State 2019, p. 418).

[7] This approach in no way implies that trafficking only occurs through international waters. In the UNODC [United Nations Office on Drugs and Crimes] (2014) report, information from law enforcement officers in Italy and Spain who specialized in organized crime and human trafficking suggests that trafficking networks utilize existing migration paths by land, sea, and air. "Victims trafficked to Spain, for instance, may fly to the main airports of the country or of neighboring countries. In the case of the land route, they will travel through the Sahel, the Sahara, to North Africa and cross the border into Ceuta or Melilla in Spain. Similarly, on the route to Italy, they will attempt the sea passage from North Africa to Lampedusa or Sicily" (UNODC [United Nations Office on Drugs and Crimes] (2014), pp. 56-57).

with the log ratio of countries' coastline length to the land area:

$$(3) \qquad (\text{Relative TIP inflow})_i = \xi + \pi z_i + \gamma_i + \mathbf{X}_i + \nu_i,$$

where z_i is the log of coastline length to the land area as a measure of border porosity in illegal entries. Higher values of z imply higher border monitoring costs and easier illegal border entries. The exclusion restriction is that z_i does not appear in Eq. (2), or that conditional on the included controls, the coastline to land area ratio has no direct effect on the modern-day pandemics other than through the opportunities and risks involved in trafficking flows. In Section 5.1, I consider a wide range of factors, including demand-side factors of illegal immigration, to weaken this assumption of the instrument's conditional exogeneity.[8]

A main endogeneity concern is that regions attracting trafficking tend to have better economic opportunities. Such places typically also have better health outcomes through stronger healthcare institutions, lowering disease mortality. To address this concern, the fatality rate is used as a placebo outcome measure throughout the study, including analyses on contact rate as a mechanism in Section 6. The trafficking risk measure should not predict lower fatality rates.

3 Preliminary Evidence

3.1 Trafficking Corridors

Fig. 2 shows three selected trafficking corridors identified by the Counter-Trafficking Data Collaborative. The COVID-19 outbreak severely hit Italy early in January 2020. By early March, Italy had 5,883 confirmed cases, compared to Austria (81), France (949), Slovenia (12), and Switzerland (268). Italy's COVID-19 numbers became a puzzle (Kuchler et al. 2022). Trafficking and illegal immigrants is a critical yet overlooked source (Rojanaworarit

[8] Another assumption on trafficking patterns, as implied in the first-stage Eq. (3), is that trafficking risk for countries persists over the years, even if annual reported (and actual) figures vary. This persistence is mainly due to the scarcity of trafficking data and the fact that the annual TIP reports often repeat the distinction between destination and source in their trafficking profiles, resulting in minimal variation over time (Fig. A1). Akee et al. (2014) provide theoretical and empirical support for the inelastic demand for trafficked persons, which may help to explain this persistence.

(a) China to North Macedonia (COVID-19)

(b) North Macedonia to Italy (COVID-19)

(c) Mexico to Switzerland (H1N1)

Fig. 2. Screenshots from the Counter-Trafficking Data Collaborative's global trafficking corridor visualizer (`https://www.ctdatacollaborative.org/map?type=corridor`). Trafficking corridors are constructed using reported numbers of trafficking cases.

and El Bouzaidi 2021). The trafficking corridor in Panel A of Fig. 2 illustrates that one of China's main outflows of trafficking is to North Macedonia. In turn, Panel B shows that one of North Macedonia's main outflows of trafficking is to Italy.

Spain had a similar crisis (Boto-García 2023). One of its primary inflow sources of trafficking comes from Bulgaria (not shown), which borders North Macedonia, a major point of transit in human trafficking (U.S. Department of State 2019). A report states that "foreign victims transiting North Macedonia are subjected to sex trafficking and forced labor in construction and agricultural sectors in Southern, Central, and Western Europe" (U.S. Department of State 2019, p. 360).

A second and more direct anecdote comes from Switzerland in the 2009 H1N1 pandemic. Besides the bordering US, Mexico's most prominent trafficking corridor is to Switzerland (Panel C of Fig. 2). Switzerland had 609 confirmed cases near the end of the pandemic compared to its bordering neighbors: Austria (192), France (880), Germany (9,213), Liechtenstein (5), and Italy (1,238). To put the numbers in perspective, by the fourth month of the pandemic in July 2009, Switzerland had the smallest population of these countries but

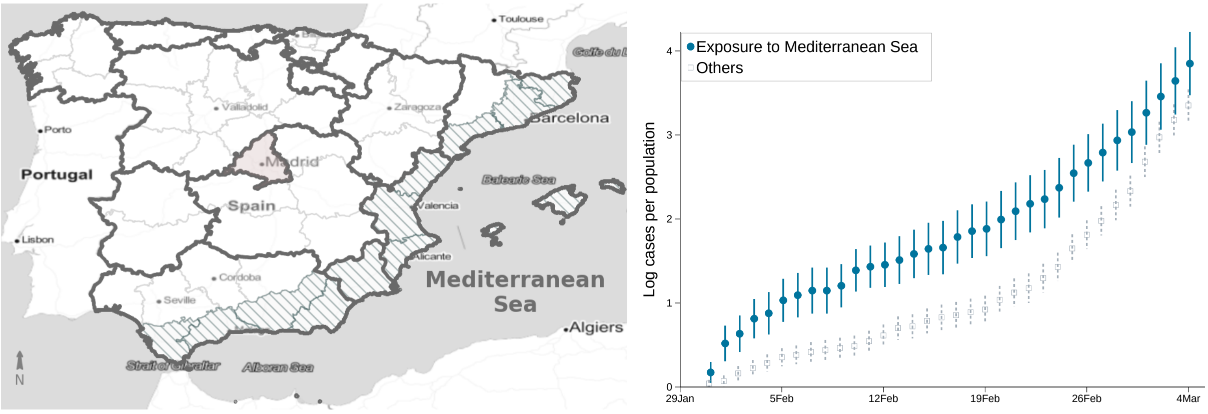

(a) PROVINCES OF SPAIN **(b)** PATH PLOT

Fig. 3. Cases per population in Spanish provinces, categorized by exposure to the Mediterranean Sea. Panel (a) shows Spain's 50 provinces (excluding Las Palmas and Santa Cruz de Tenerife in the Canary Islands). The capital, Madrid, is in pink. The twelve provinces along the Mediterranean Sea, facing the northern coast of Africa, are shaded in blue. Panel (b) displays model-free path plots of the daily log cumulative COVID-19 cases per population based on province-day data for Feb–Mar 2020, comparing these twelve sea-facing provinces (in blue) to all other provinces. Vertical lines represent standard errors of the mean.

the highest number of confirmed cases per population.[9]

3.2 Spanish Provinces and the Mediterranean Sea

The implied mechanism with coastlines as an instrumental variable (Section 2.4) is that longer coastlines are harder to monitor, increasing the risk of trafficking inflows. This section provides model-free evidence that Spanish provinces exposed to the Mediterranean Sea had higher cases per population early in the COVID-19 pandemic.

A common trafficking route by sea involves the Mediterranean Sea, with trafficking networks exploiting this route to bring illegal migrants into Europe (U.S. Department of State 2018, p. 407). A large proportion (more than 90 percent) of Mediterranean crossings originate from Libya, a primary departure point for vulnerable migrants from and transiting Libya en route to Europe (U.S. Department of State 2017, p. 432). Spain, for instance, has their victims "moved by sea into Southern Spain" (U.S. Department of State 2018, p. 394), and experiences an "increasing number of victims arrived in southern Spain by sea via Morocco" (U.S. Department of State 2019, p. 432).

Based on such reports, I examine whether Spanish provinces closer to the Mediterranean Sea, a common trafficking route (UNODC [United Nations Office on Drugs and

[9] Section 5.1 considers higher reported cases potentially arising from more stringent testing in the COVID-19 pandemic.

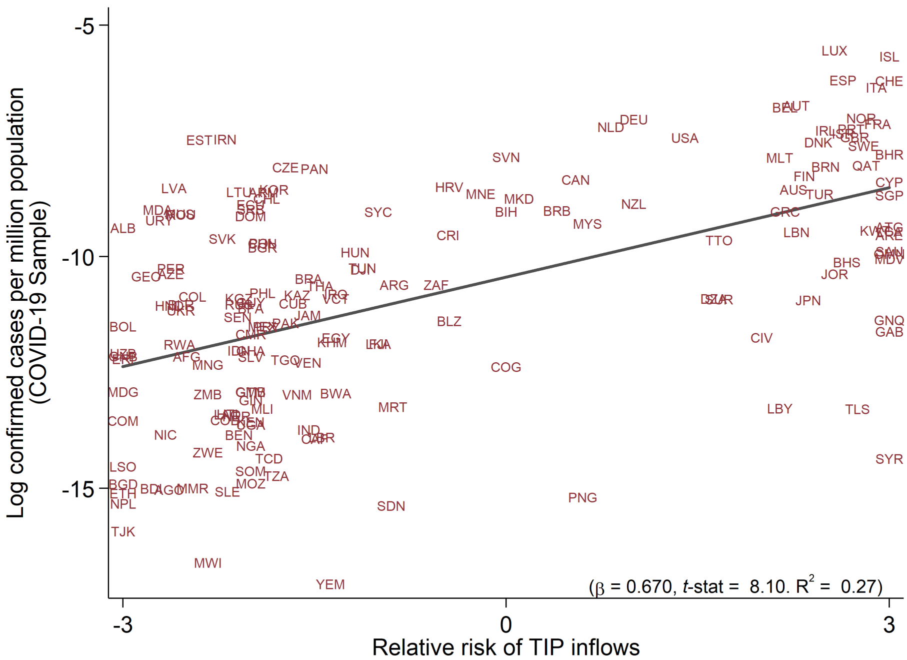

Fig. 4. OLS relationship: Trafficking risk and the COVID-19 pandemic. Log confirmed cases per million population as of March 2020 and trafficking risk. The graph "soft-censors" the top five percent of confirmed cases. Fig. B1 replicates this for the H1N1 pandemic.

Crimes] 2018), have more cases per population. Fig. 3a shows the twelve provinces on the eastern and southern side exposed to the Mediterranean Sea, including Cadiz, which is close to Ceuta and Melilla, a common land route of trafficking from Africa into Spain. Fig. 3b confirms that the twelve Spanish provinces exposed to the Mediterranean Sea have more cases per population than the other Spanish provinces.[10]

3.3 OLS Findings

Fig. 4 illustrates the cross-country connection between trafficking risk and COVID-19 cases. Estimating Eq. (2) using the combined H1N1 and COVID-19 samples confirms this association. Adjusting for the disease dummies, region dummies, and proximity to source countries (Section 2.3), the statistically significant estimate of 0.45 (Table B1) implies an economically meaningful change.

For a sense of magnitude, I compare three European countries with varying levels of trafficking inflow risk: Bulgaria (low), Bosnia (mid), and Belgium (high). Bulgaria has a trafficking measure of -1.9 (approximately the 25th percentile). Bosnia has a measure of

[10] The twelve provinces are Alicante, Almeria, Islas Baleares, Barcelona, Castellon, Cadiz, Girona, Granada, Murcia, Malaga, Tarragona, and Valencia. For a dedicated study on Spain, please see Boto-García (2023), who finds that southern Mediterranean provinces exhibit a stronger link between mobility flows and COVID-19 cases.

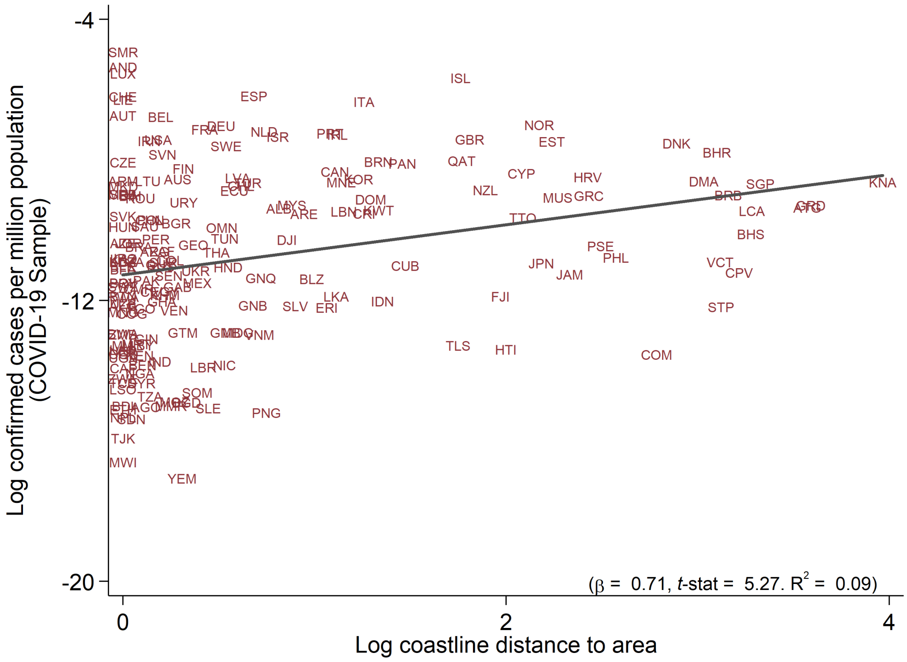

Fig. 5. Reduced-form relationship: Trafficking risk and the COVID-19 pandemic. Log confirmed cases per million population as of March 2020 and the log coastline length to area. The graph "soft-censors" the top five percent of confirmed cases. Fig. B2 replicates this for the H1N1 pandemic.

0 (approximately the 60th percentile). The estimate of 0.45 implies that the difference between these two countries' cases is 1.35 times ($e^{1.9\times0.45}-1$). On the higher end, I compare Bosnia to Belgium, which has a trafficking measure of 2.18 (approximately the 75th percentile). The estimate of 0.45 implies that the difference in pandemic severity is 1.66 times ($e^{2.18\times0.45}-1$).

Fig. 5 confirms the reduced-form connection between coastlines and COVID-19 cases. Section 4 re-examines the non-causal association in Fig. 4 using coastlines as a plausibly exogenous instrument of trafficking (Section 2.4).

4 Results

4.1 Confirmed Cases per Capita

Table 1 reports the two-stage least-squares estimates of the Eq. (2) with the log of coastline length to the land area as the instrument for the relative trafficking inflow risk measure (Section 2.4). The outcome variables in Table 1 are case records by the 3rd month into the pandemic, the earliest month with relatively complete data (Section 2.1). Panel A reports the 2SLS estimates. Panel B reports the first stages. Column (1) shows a positive and

Table 1
Trafficking risk and confirmed cases: 2SLS estimates

	(1)	(2)	(3)	(4)	(5)	(6)	(7)	(8)	(9)
	A. Two-Stage Least Squares								
							Placebo outcomes		
	Dep. var. is log confirmed cases (per million population)						Dep. var. are log of		
							CFR	CDR	Deaths
Relative TIP flow	1.09^{***}	1.45^{***}	1.48^{***}	1.48^{***}	1.67^{***}	1.03^{***}	–0.13	1.35^{***}	–0.13
	(0.23)	(0.28)	(0.31)	(0.30)	(0.48)	(0.26)	(0.12)	(0.30)	(0.09)
Covid-19 dummy		4.38^{***}	4.54^{***}	3.86^{***}			-2.76^{***}	1.61^{**}	-0.88^{***}
		(0.37)	(0.32)	(0.39)			(0.14)	(0.65)	(0.25)
Contiguity dummy				0.13	-2.48^{**}	–0.77	0.22	0.20	–0.32
				(0.78)	(1.11)	(0.86)	(0.43)	(0.68)	(0.27)
Common language dummy				0.52	0.86	1.18	-0.91^{***}	–0.27	-0.48^{*}
				(0.71)	(1.21)	(1.10)	(0.33)	(0.73)	(0.26)
Distance from Gzero				-0.10^{*}	0.21	-0.29^{*}	0.03	-0.08^{*}	0.01
				(0.05)	(0.22)	(0.17)	(0.02)	(0.05)	(0.02)
PTA dummy				-1.37^{***}	-1.47^{**}	1.71^{***}	-0.83^{***}	-2.12^{***}	-0.56^{***}
				(0.48)	(0.69)	(0.64)	(0.17)	(0.46)	(0.16)
Log confirmed cases								–0.11	0.61^{***}
								(0.12)	(0.05)
First-stage F-stat	26.44	24.97	22.05	23.94	7.32	25.01	23.94	24.56	24.56
	B. First Stage								
	Dep. var. is relative TIP inflow								
Log coastline to area	0.61^{***}	0.60^{***}	0.61^{***}	0.62^{***}	0.55^{***}	0.70^{***}	0.62^{***}	0.32^{**}	0.62^{***}
	(0.12)	(0.12)	(0.13)	(0.13)	(0.20)	(0.14)	(0.13)	(0.14)	(0.12)
	C. Ordinary Least Squares								
	Dep. var. is log confirmed cases (per million population)								
Relative TIP flow	0.45^{***}	0.53^{***}	0.46^{***}	0.46^{***}	0.45^{***}	0.41^{***}	-0.09^{**}	0.03	–0.01
	(0.08)	(0.06)	(0.06)	(0.05)	(0.07)	(0.08)	(0.04)	(0.04)	(0.03)
Region dummies	—	—	Yes	Yes	Yes	Yes	Yes	Yes	Yes
Gravity controls	—	—	—	Yes	Yes	Yes	Yes	Yes	Yes
Sample	Both	Both	Both	Both	H1N1	COVID-19	Both	Both	Both
Countries	174	174	174	174	135	168	174	174	174
Observations	303	303	303	303	135	168	303	303	303

Notes—Panel A reports the two-stage least-squares estimates, using the log coastline length to the land area as the instrument for trafficking risk (relative TIP flow, Section 2.2). The dependent variable in columns (1)–(6) of Panel A is the log of confirmed cases of the diseases per million population by the third month into the pandemic. Columns (2)–(4) incrementally add the COVID-19 dummy, the region dummies, and the proximity controls to the source country of the pandemic (Section 2.3). Columns (5) and (6) estimate the two pandemics separately. Columns (7)–(9) report placebo outcomes: the log of the case fatality rate (CFR), defined as confirmed deaths divided by confirmed cases, in (7); the log of the crude death rate, defined as confirmed deaths divided by population, in (8); and the log of confirmed deaths in (9). Panel B reports the corresponding first-stage results. Panel C reports the analogous OLS estimates. All panels include the same set of covariates but are not always reported to conserve space. Standard errors in parentheses. *** $p < 0.01$, ** $p < 0.05$, * $p < 0.1$.

significant relationship between pandemic severity and the trafficking risk measure, with a first-stage heteroskedastic-robust F-statistic of 26. Columns (2)–(4) incrementally add the COVID-19 dummy, the region dummies, and the proximity controls to the source country of the pandemic (Section 2.3).

The 2SLS estimates are larger than the OLS estimates (Panel C), potentially arising from measurement error in the trafficking risk measure biasing the OLS estimates downwards.[11] The overall results replicate separately in both of the pandemic episodes (column (5) for H1N1, column (6) for COVID-19), with smaller effect sizes for COVID-19. Fig. 6 replicates to the different months for both pandemics.

[11] As anticipated, performing the Hausman test using model (4) rejects the null hypothesis that the trafficking measure is exogenous, indicating that the OLS estimates are inconsistent.

While Section 2.4 establishes a case for coastlines as an instrument for trafficking, the assumptions for its validity may be violated and cannot be tested directly. As part of an extensive set of robustness, Section 5 considers four additional sets of control variables to weaken the conditional exogeneity assumption of the instrument, over-identification tests, and placebo IV tests. The following subsection considers placebo outcomes in the same setup.

4.2 Fatality Rates as Placebo Outcomes

A key concern around endogeneity is that regions with higher trafficking inflows have better economic opportunities (Bales 2007; Cho 2015). These regions are more urbanized and well-connected, potentially leading to greater transmission rates. However, these countries should have lower fatality rates to the extent that the strength of their healthcare institutions buffers against disease mortality. Therefore, I use the case fatality rate as a placebo outcome to test whether such endogeneity drives the result.

Columns (7)–(9) of Table 1 present evidence against this endogeneity concern using the placebo outcomes. The outcome variable in column (7) is the case fatality rate (CFR, deaths divided by confirmed cases). While the estimate is negative, it is non-significant. The estimate for the (CDR, deaths per capita) in column (8) is positive and statistically significant, running against the hypothesis that trafficking is positively correlated to better healthcare institutions. Finally, the estimate for deaths in column (9) is non-significant. Overall, the placebo outcomes do not suggest that the trafficking risk measure simply captures more developed institutions, a finding replicated in the other months (Fig. 6).

5 Robustness

5.1 Additional Controls

This section considers four extensive sets of additional controls to weaken the conditional exogeneity assumption of the coastline instrument. These revolve around (i) international movement, (ii) health and institutional factors, (iii) social and cultural factors, and (iv) geo-

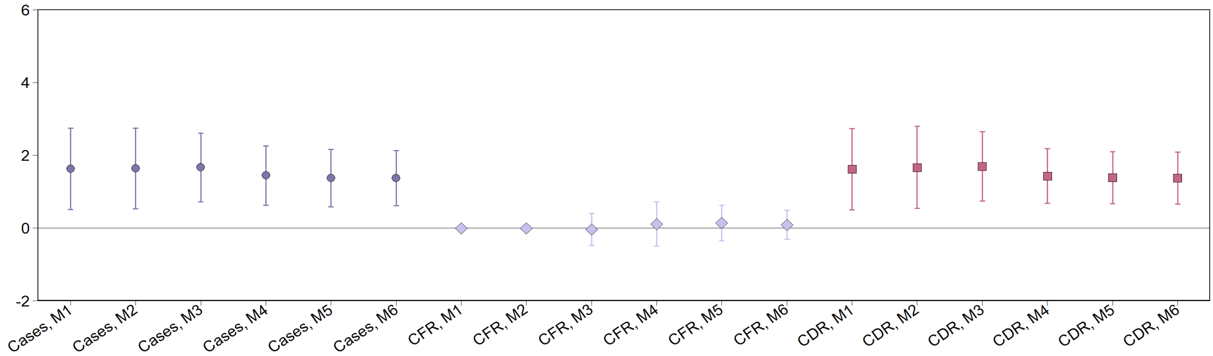

(a) H1N1 Sample

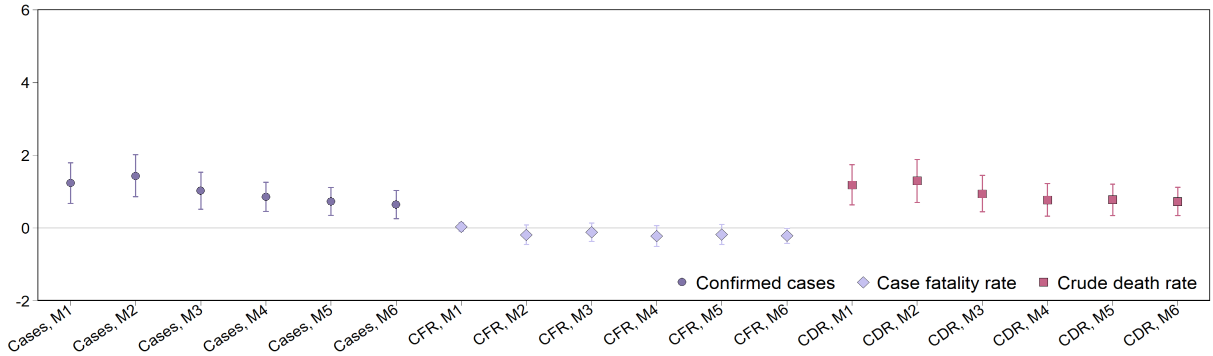

(b) COVID-19 Sample

Fig. 6. Two-Stage Least Squares (2SLS) estimates by month and pandemic. This figure presents the 2SLS estimates with cumulative confirmed cases as the dependent variable, measured from the 1st to the 6th month of the pandemic. The specification follows column (4) of Table 1. Capped vertical bars indicate the 95% confidence interval.

graphical factors. Broadly, these include demand- and supply-side determinants of human trafficking inflow and illegal entries that are potentially linked to pandemic severity. Overall, with an extensive set of additional controls, the 2SLS estimate decreases in magnitude but remains statistically significant.

First, the coastline-to-area instrument may capture other official movement factors unrelated to trafficking and irregular immigration. Table C1 estimates the 2SLS results with an additional set of controls for tourism and regular migration, including overall regular migration inflow from source countries, overall migration, asylum and refugee seekers, and tourism. Overall, the 2SLS estimate drops to 0.74 with all the above controls included.

Second, Table C2 considers a set of health and institutional factors plausibly linked to pandemic severity (Aizenman et al. 2022). These include anti-trafficking standards, polity and constraint on executive measures, GDP (Gross Domestic Product) per capita, government size, government health expenditure per capita, number of tests conducted (only for COVID-19, Mathieu et al. 2020), and health measures such as old-age dependency (ratio of above 64 to working-age population) and immunization rates. The 2SLS estimates tend to be smaller than those in Table 1 but remain statistically significant except with the log health expenditure per capita measure, which is highly correlated with the trafficking measure in the first stage. The first stage becomes very weak when including the log health expenditure per capita measure, with an F-statistic of 3.0, leading to an insignificant second-stage estimate ($p < .1$).[12] The 2SLS estimate drops to 0.71 with all the above controls included (except for test numbers, which are only available for COVID-19).

Third, Table C3 considers social and cultural factors. These additional controls include religious composition (percentage of Protestant, Muslim, and Roman Catholic), ethnolinguistic fragmentation,[13] size of government welfare, school enrollment rates,[14] mass mobilizations coinciding with the pandemics (Clark and Regan 2016), population density, and urbanization. The 2SLS estimate drops to 0.56 with all the above controls included.

Lastly, Table C4 considers geographical factors, which are potentially correlated with both risk of trafficking inflows and other economic-related factors (e.g., Bloom et al. 1998; Gallup et al. 1999; Dell et al. 2012; Nunn and Puga 2012). These include island and landlocked dummies, (absolute) latitude, mean temperatures, humidity, and soil quality/climate variables.[15] When all controls are added, the 2SLS estimate attenuates to 0.81.

5.2 Overidentification Tests

This section uses measures of drug trafficking as alternative instruments in overidentification tests to assess the validity of the coastline instrument. I consider drug trafficking as an alternative instrument because of its close links to human trafficking (UNODC [United Nations Office on Drugs and Crimes] 2011).[16] The test statistic is the Hansen test statis-

[12] The Anderson-Rubin Wald test, robust to a weak first stage, yields a χ^2-test statistic of 40.8 and a p-value < .0001, rejecting the null hypothesis that the trafficking risk measure is statistically equal to zero. This indicates that the expected association between trafficking and pandemic numbers persists, even with a weak first stage.

[13] Ethnolinguistic fragmentation has been linked to trafficking flows (Akee et al. 2010), social trust during a pandemic (Amdaoud et al. 2021), and economic growth (Easterly and Levine 1997).

[14] Higher secondary school enrollment has higher confirmed cases per population (Table C3).

[15] The coefficients for latitude and mean temperatures are consistent with studies finding that the hotter climates in regions further from the equator impede the spread of local epidemics (Bloom-Feshbach et al. 2013; Ma et al. 2020; Wang et al. 2020, 2021).

[16] A link between drug and human trafficking involves both routes and people, with UNODC [United Nations Office on Drugs and Crimes] (2011) noting a "connection between the smuggling of migrants and the rapidly growing trade in cocaine across the Sahara to North Africa and Europe. In 2005, there were already indications

tic, for the null that the instruments are uncorrelated with the error term in the structural equation.

The three alternative instruments are (i) the log of cocaine seizures in a country per capita, (ii) log cocaine inflow per capita, and (iii) log amphetamine (-type stimulants) inflow per capita. These data come from the Individual Drug Seizures data (UNODC [United Nations Office on Drugs and Crimes] 2020, Table A1).

The Hansen tests never reject the null hypothesis that the overidentification restrictions are valid (Table D1). I also consider an alternative version of this test, with the coastline measure included as a regressor in the structural equation. If the coastline instrument is valid, it should not be statistically significant. This is because a valid instrument is supposed to predict the endogenous variable (through the first stage) but not be correlated with the error term in the structural equation (the second stage). The test confirms that the coastline variable is never statistically significant (Table D1). I emphasize that the overidentification tests do not definitively validate the coastline instrument, as the tests themselves rest on the assumption that the alternative instruments are valid.

5.3 Falsification Tests with Placebo Instruments

Finally, I consider a set of variables that, while theoretically invalid as instruments, might capture the same endogenous factors as the coastline instrument. These placebo instruments, similar in spirit to negative controls (Lipsitch et al. 2010), would challenge the validity of the main instrument if they produce similar 2SLS estimates and capture the same underlying unobserved and endogenous factors.

Table 2 presents these falsification tests. While GDP per capita is unlikely to meet the exclusion restriction, using it as a placebo instrument leads to a positive and significant 2SLS estimate.[17] This raises concerns about the main 2SLS estimates (Section 4). If GDP per capita captures the same underlying endogenous factors as those by the coastlines instrument, it may mean the coastlines instrument is invalid. Conversely, GDP per capita may reflect economic conditions that influence both the prevalence of trafficking and the

that some migrants were trading small quantities of cocaine over the Sahara" (UNODC [United Nations Office on Drugs and Crimes] 2011, pp.46–47).

[17] This differs from controlling for it in the regressions (as in Section 5.1).

Table 2
Placebo tests for the coastline instrument

	(1)	(2)
Instrumenting the trafficking risk measure using	2SLS estimate	2SLS estimate t-statistic
Log GDP per capita	0.84***	(9.21)
Log GDP	–1.93	(–0.73)
Log migration inflow	–2.76	(–0.58)
Log refugee inflow	–1.00	(–1.05)
Log tourism arrivals	0.39	(1.26)
Log refugee stock	–1.73	(–0.82)
Log population living in urban areas	1.54***	(3.95)
Log total fisheries production	1.67	(1.14)

Notes—Each row presents a 2SLS regression (Eq. (2)) with the row variable as the instrument for the trafficking risk (relative TIP inflow, Eq. (1)). All regressions otherwise follow column (4) of Table 1. t-statistics are heteroskadasticity robust. *** indicates significance at the 1 percent level.

severity of the pandemic (e.g., Bales 2007; Cho et al. 2013). The 2SLS estimate using GDP is not significant.

Using migration and refugee inflow as instruments does not lead to a detectable effect of the trafficking inflow risk measure, suggesting that the coastline porosity measure is not just capturing broader irregular migration patterns. I also consider urbanization since countries with relatively smaller areas have higher urbanization. Using urbanization leads to a statistically significant second stage but does not invalidate the main 2SLS results in that the first-stage and reduced forms have the wrong signs (urbanization is negatively correlated with the trafficking measure and case numbers). The remaining variables mitigate concerns that the coastline instrument inadvertently captures other factors: refugee stock and flow, the size of the tourism industry, and the fishery industry (as a coast-related informal sector). As with Section 5.1, these tests are somewhat open-ended, with some suggesting a failure of falsification, e.g., with GDP.

5.4 Additional Robustness Tests

The main measure of trafficking inflow risk (Eq. (1)) depends on the incidence of trafficking outflow. Appendix E additionally show that a measure of trafficking inflow risk independent of outflow incidence, i.e., just considering the destination indicator (as opposed to the ratio of destination to source indicators in Eq. (1)), does not materially change the findings (Fig. E1). This applies to different months and the two pandemics (Appendix E).

While Section 2.4 lays out the international policy concerns with policing land and sea borders, the coastline instrument might not be a uniformly good predictor of trafficking inflow across all countries or regions. In Appendix E, I perform a regional jackknife to test if certain regions disproportionately drive the observations. Iteratively, leaving out one of the 13 regions does not substantially affect the estimates. However, the standard errors nearly double when excluding the (Northern and Western) European countries (Fig. E2).

6 Contact Rate as Mechanism

This section examines a specific mechanism through which trafficking is linked to disease spread. The potential mechanism relates to the vulnerable circumstances of irregular migrants. Once within borders, they are less likely to seek medical aid and self-quarantine because of lower health literacy and adverse living and working conditions (Bojorquez et al., 2021; Rojanaworarit and El Bouzaidi, 2021; Todres and Diaz, 2021; Rojanaworarit and El Bouzaidi, 2022). These vulnerable circumstances can lead to higher transmission in the general population (Chinazzi et al. 2020; Rojanaworarit and El Bouzaidi 2021; Todres and Diaz 2021).

6.1 SIRD Model

To test higher contact rates as a channel, I employ a regression model derived from well-established Susceptible-Infectious-Recovered-Deceased (SIRD) principles. Specifically, I model trafficking as proportionally increasing the contact rate (Allcott et al. 2024). I make the simplifying assumption that the number of susceptible individuals closely approximates the total population size (Allcott et al. 2024). This assumption is most tenable in the early months, even in cases with extremely high numbers of infections (the infected, recovered, and deceased) such that the number of susceptible individuals differs more drastically from the total population size (Appendix F). This approach yields a SIRD-derived model (Eq. (4)), which I take to high-frequency COVID-19 data for the testable hypothesis that trafficking increases spread through increasing contact rates.

$$\log\left(\mathrm{C}_{i,t+1} - \mathrm{C}_{it}\right) = \pi_0 + \tau(\text{Relative TIP inflow})_i + \pi_1 \log(\hat{\mathrm{I}}_{it}) + \mathbf{\Pi}_t \mathbf{X}_{it} + \xi_{it} \tag{4}$$

Eq. (4) models the log of cumulative changes in cases over weeks as dependent on the trafficking risk measure and the log of the simulated cumulative stock of infected individuals ($\hat{\mathrm{I}}_{\mathrm{it}}$). $\hat{\tau}$ captures whether trafficking risk predicts an increase in cases and can also be interpreted as the estimated proportional increase in the contact rate (Appendix F). C_{it} is the stock of COVID-19 cases in week t in country i (Hale et al. 2021). $\hat{\mathrm{I}}_{\mathrm{it}}$ is the stock of infected cases based on the SIRD model, simulated using a few combinations of the SIRD parameters (Appendix F). $\mathbf{X}_{\mathbf{it}}$ in Eq. (4) also includes the COVID-19 government response stringency indices and the economic support indices (Hale et al. 2021) to control for non-pharmaceutical interventions,[18] week fixed effects, country fixed effects, and the region-by-week fixed effects. Standard errors are clustered at the country level. Please see Appendix F for the SIRD foundations and assumptions behind Eq. (4).

Taking Eq. (4) to the high-frequency panel data yields four testable hypotheses. First, if the mechanism holds, $\hat{\tau}$ should be positive and statistically significant. Second, this positive association should attenuate in later months once: (a) individuals internalize the health risks of the pandemic and voluntarily practice safe distancing, and (b) public health officials start imposing movement restrictions (stringency indices at the country-week level are included as controls). Third, and as a form of validation of the SIRD modeling in Eq. (4), $\hat{\pi}_1$ should statistically be equal to 1 so that the increase in infections is directly proportional to the increase in the growth of cases per capita (Appendix F). Fourth, and as a placebo test, the trafficking risk measure should not predict lower fatality rates.

6.2 Results

Estimating Eq. (4) broadly verifies the above. Fig. 7 visualizes two sets of the coefficients for the growth in cases per capita (Table G3) and the fatality rate (Table G6). From the OLS estimates, the trafficking risk measure is positive and statistically significant only in the first three months of pooled observations (Jan–Mar, Table G1), but not in later months (Apr-Dec, Table G2). Fig. 7a shows that modeling the trafficking measure by the individual months confirms the above observations, with the estimate statistically significant in March. This is consistent with illegal immigration substantially decreasing as economic

[18] Economic support, for instance, might affect individuals' decisions to seek work despite health risks.

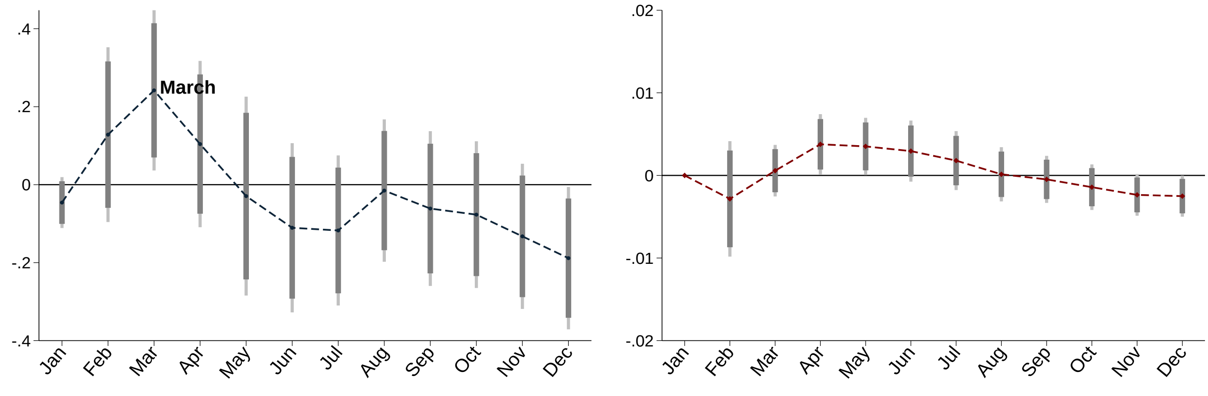

(a) $\log(C_t - C_{t-1})$ **(b)** Case fatality rate

Fig. 7. Estimated coefficients of trafficking risk (Eq. (1)) by months on case growth and fatality rate. Estimates are from Table G3 for cases and Table G6 for fatality rate (γ = 1⁄12, R_0 = 3, and μ = 0.01). Vertical bars are 95% confidence intervals.

opportunities dry up with forced closures.

Using the estimate for Jan–Mar in column (1) of Table G1 of 0.19 (and reusing the examples from Section 3.3 to access magnitudes) implies that going from approximately the 25th percentile to the 60th percentile in the trafficking inflow risk measure increases contact rate by a factor of 0.43 ($e^{1.9\times0.19} - 1$) in the early months while going from approximately the 60th percentile to the 75th percentile increases contact rate by a factor of 0.51 ($e^{2.18\times0.19} - 1$).

In most specifications, $\hat{\pi}_1$ is not statistically different from 1, confirming that Eq. (4) respects the fundamental SIRD dynamics.[19] In placebo regressions using fatality rate as the outcome, the $\hat{\tau}$ coefficient is statistically zero in most specifications and never negative (Tables G4 to G6). Instrumenting the trafficking risk measure with coastline instruments in the first stage (Tables G7 to G12) broadly corroborates the above OLS results, with trafficking risk increasing contact rate only in the earlier months (Feb), and never predicting lower fatality rates.

Overall, the SIRD-based regression results are consistent with trafficking risk increasing disease spread through an increase in contact rates. In the earlier months (Feb–Mar) of the COVID-19 pandemic, countries with higher trafficking risk have as much as a 50 percent increase in contact rate compared to countries closer to the median in trafficking risk.

[19] The exceptions are in models for the later periods when the assumption that the susceptible population approximates the entire population becomes less tenable.

7 Conclusion

The literature on the spread of pandemics has predominantly focused on official travel. This study sheds light on a critical yet overlooked factor—illegal immigration (Rojanaworarit and El Bouzaidi 2021). Examining COVID-19 data on the number of cases and fatality rate, I find that countries with higher trafficking inflow risk have higher per capita infections. This pattern replicates in the H1N1 pandemic. Using the coastlines-to-area ratio as an exogenous instrument for trafficking risk, I obtain similar conclusions, suggesting a causal interpretation. Importantly, I also find that trafficking inflow risk does not predict lower fatality rates.

To test whether increased contact rates serve as a channel through which trafficking risk increases transmissions, I theoretically model trafficking as augmenting the contact rate using dynamics implied within the SIRD framework. With reasonable assumptions to simplify the augmented SIRD model for tractability, it reduces to an estimable model. I then take the model to high-frequency COVID-19 country-week panel data of case numbers and COVID-19 government response stringency measures. The data suggests that trafficking risk increases cases per population through the contact rate, but only in the earlier months (Feb–Mar). As falsification tests, trafficking risk never predicts lower fatality rates. This timing that trafficking risk increases cases only in the earlier months is consistent with disappearing economic opportunities (Boto-García 2023) and hints at the value of lockdowns to cut contact rates.

It is worth noting the limitations. Trafficking routes often overlap with illegal immigration pathways, as both involve the movement of vulnerable populations across borders, often under exploitative conditions and organized crime. However, most illegal immigration and trafficking are untracked, which means that the data is likely noisy and biased. Moreover, trafficking incidence might capture unobserved factors that determine the severity of the pandemic. The unbiasedness of the estimate rests on the extent to which the identifying assumption that coastline variation is an exogenous instrument is valid and the extent to which the extensive set of robustness and falsification tests rule out alternate explanations. Nonetheless, it is helpful to interpret the results with caution. More granular within-country data is likely to offer better identification opportunities. Future research could explore alternative methods or data to further investigate the mechanisms at play.

Overall, countries with higher trafficking incidence tend to have more severe outbreaks. The evidence that trafficking only increases the rise in cases through contact rates in the early months of the pandemic reinforces the value of timely state-imposed lockdowns and self-isolation. On the other hand, social inequalities left trafficked migrants particularly vulnerable during the pandemic (Bojorquez et al., 2021; Rojanaworarit and El Bouzaidi, 2021; Todres and Diaz, 2021). This research, therefore, also exposes potential gaps in public health systems that must be bridged to ensure resilient future pandemic responses.

References

Abel, G. J. and J. E. Cohen (2019). Bilateral international migration flow estimates for 200 countries. *Scientific Data 6*(1), 82. 7, 29, 34

Acemoglu, D., S. Johnson, and J. A. Robinson (2001). The colonial origins of comparative development: An empirical investigation. *American Economic Review 91*(5), 1369–1401. 29, 33, 37

Adda, J. (2016). Economic activity and the spread of viral diseases: Evidence from high frequency data. *The Quarterly Journal of Economics 131*(2), 891–941. 5

Aizenman, J., A. Cukierman, Y. Jinjarak, S. Nair-Desai, and W. Xin (2022). Gaps between official and excess covid-19 mortality measures: The effects of institutional quality and vaccinations. *Economic Modelling 116*, 105990. 17

Akee, R., A. K. Basu, A. Bedi, and N. H. Chau (2014). Transnational trafficking, law enforcement, and victim protection: A middleman trafficker's perspective. *The Journal of Law and Economics 57*(2), 349–386. 10

Akee, R. K. Q., A. K. Basu, N. H. Chau, and M. Khamis (2010). Chapter 28 ethnic fragmentation, conflict, displaced persons and human trafficking: An empirical analysis. In *Frontiers of Economics and Globalization*, Frontiers of economics and globalisation, pp. 691–716. Emerald Group Publishing Limited. 18

Allcott, H., L. Boxell, J. Conway, B. Ferguson, M. Gentzkow, and B. Goldman (2024). What explains temporal and geographic variation in the early us covid-19 pandemic? Available at SSRN: `https://ssrn.com/abstract=3610422` or `http://dx.doi.org/10.2139/ssrn.3610422`. 21, 40

Amdaoud, M., G. Arcuri, and N. Levratto (2021). Are regions equal in adversity? A spatial analysis of spread and dynamics of COVID-19 in Europe. *European Journal of Health Economics 22*(4), 629–642. 18

Bales, K. (2007). What predicts human trafficking? *International Journal of Comparative and Applied Criminal Justice 31*(2), 269–279. 3, 16, 20

Beverelli, C. and G. Orefice (2019). Migration deflection: The role of preferential trade agreements. *Regional Science and Urban Economics 79*, 103469. 7

Bloom, D. E., J. D. Sachs, P. Collier, and C. Udry (1998). Geography, demography, and economic growth in Africa. *Brookings Papers on Economic Activity 1998*(2), 207–295. 18

Bloom-Feshbach, K., W. J. Alonso, V. Charu, J. Tamerius, L. Simonsen, M. A. Miller, and C. Viboud (2013). Latitudinal variations in seasonal activity of influenza and respiratory syncytial virus (RSV): A global comparative review. *PLOS ONE 8*(2), 1–12. 18

Bogoch, I. I., O. J. Brady, M. U. G. Kraemer, M. German, M. I. Creatore, M. A. Kulkarni, J. S. Brownstein, S. R. Mekaru, S. I. Hay, E. Groot, A. Watts, and K. Khan (2016). Anticipating the international spread of zika virus from Brazil. *The Lancet 387*(10016), 335–336. 2, 5

Bojorquez, I., B. Cabieses, C. Arósquipa, J. Arroyo, A. C. Novella, M. Knipper, M. Orcutt, A. C. Sedas, and K. Rojas (2021). Migration and health in latin america during the COVID-19 pandemic and beyond. *The Lancet 397*(10281), 1243–1245. 2, 4, 21, 25

Boto-García, D. (2023). Investigating the two-way relationship between mobility flows and covid-19 cases. *Economic Modelling 118*, 106083. 2, 5, 11, 13, 24

Chinazzi, M., J. T. Davis, M. Ajelli, C. Gioannini, M. Litvinova, S. Merler, A. P. y Piontti, K. Mu, L. Rossi, K. Sun, C. Viboud, X. Xiong, H. Yu, M. E. Halloran, I. M. Longini, and A. Vespignani (2020). The effect of travel restrictions on the spread of the 2019 novel coronavirus (COVID-19) outbreak. *Science 368*(6489), 395–400. 2, 4, 5, 21

Chiswick, B. R. and P. W. Miller (2015). Chapter 5 - International migration and the economics of language. In B. R. Chiswick and P. W. Miller (Eds.), *Handbook of the Economics of International Migration*, Volume 1 of *Handbook of the Economics of International Migration*, pp. 211–269. North-Holland. 7

Cho, S.-Y. (2015). Modeling for determinants of human trafficking: An empirical analysis. *Social Inclusion 3*(1), 2–21. 3, 16

Cho, S.-Y., A. Dreher, and E. Neumayer (2013). Does legalized prostitution increase human trafficking? *World Development 41*, 67–82. 20

Clark, D. and P. Regan (2016). Mass Mobilization Protest Data. 18, 29, 36

Cunningham, S., G. DeAngelo, and B. Smith (2020). Fracking and risky sexual activity. *Journal of Health Economics 72*, 102322. 5

Dell, M., B. F. Jones, and B. A. Olken (2012). Temperature shocks and economic growth: Evidence from the last half century. *American Economic Journal: Macroeconomics 4*(3), 66–95. 18

Diamond, J. M. (1997). *Guns, Germs, and Steel: The Fates of Human Societies*. New York: W.W. Norton & Company. 5

Djemai, E. (2018). Roads and the spread of HIV in Africa. *Journal of Health Economics 60*, 118–141. 5

Docquier, F., C. Vasilakis, and D. Tamfutu Munsi (2014). International migration and the propagation of HIV in sub-Saharan Africa. *Journal of Health Economics 35*, 20–33. 5

Easterly, W. and R. Levine (1997). Africa's growth tragedy: Policies and ethnic divisions. *The Quarterly Journal of Economics 112*(4), 1203–1250. 18, 29, 36

Fang, H., L. Wang, and Y. Yang (2020). Human mobility restrictions and the spread of the novel coronavirus (2019-nCoV) in China. *Journal of Public Economics 191*, 104272. 2, 5

Ferguson, N. M., D. A. T. Cummings, C. Fraser, J. C. Cajka, P. C. Cooley, and D. S. Burke (2006). Strategies for mitigating an influenza pandemic. *Nature 442*(7101), 448–452. 2

Frank, R. W. (2013). Human trafficking indicators, 2000-2011: A new dataset. 2, 6, 29, 30

Gallup, J. L., J. D. Sachs, and A. D. Mellinger (1999). Geography and economic development. *International Regional Science Review 22*(2), 179–232. 18

Gurevich, T. and P. Herman (2018). The dynamic gravity dataset: 1948–2016. USITC Working Paper 2018-02-A, United States International Trade Commission. 7, 29, 32, 37

Hale, T., N. Angrist, R. Goldszmidt, B. Kira, A. Petherick, T. Phillips, S. Webster, E. Cameron-Blake, L. Hallas, S. Majumdar, and H. Tatlow (2021). A global panel database of pandemic policies (Oxford COVID-19 Government Response Tracker). *Nature Human Behaviour 5*(4), 529–538. 22, 42, 43, 44, 45, 46, 47

Khan, K., R. Eckhardt, J. S. Brownstein, R. Naqvi, W. Hu, D. Kossowsky, D. Scales, J. Arino, M. MacDonald, J. Wang, J. Sears, and M. S. Cetron (2013). Entry and exit screening of airline travellers during the A(H1N1) 2009 pandemic: A retrospective evaluation. *Bulletin of the World Health Organization 91*(5), 368–376. 2, 5

Khan, S. and S. B. Singh (2014). The economics of Transnational Organised Crime (TOC) in the maritime domain: Drug trafficking in Africa and the southern African continent. *Journal of Social Sciences 41*(3), 523–534. 2

Kiss, L. and C. Zimmerman (2019). Human trafficking and labor exploitation: Toward identifying, implementing, and evaluating effective responses. *PLOS Medicine 16*(1), e1002740. Editorial. 2

Kraemer, M. U. G., C.-H. Yang, B. Gutierrez, C.-H. Wu, B. Klein, D. M. Pigott, O. C.-. D. W. Group†, L. du Plessis, N. R. Faria, R. Li, W. P. Hanage, J. S. Brownstein, M. Layan, A. Vespignani, H. Tian, C. Dye, O. G. Pybus, and S. V. Scarpino (2020). The effect of human mobility and control measures on the COVID-19 epidemic in China. *Science 368*(6490), 493–497. 2, 5

Kuchler, T., D. Russel, and J. Stroebel (2022). JUE Insight: The geographic spread of COVID-19 correlates with the structure of social networks as measured by facebook. *Journal of Urban Economics 127*, 103314. JUE Insights: COVID-19 and Cities. 5, 10

La Porta, R., F. Lopez-de Silanes, A. Shleifer, and R. Vishny (1999). The quality of government. *Journal of Law, Economics, and Organization 15*(1), 222–279. 29, 36

Li, R., S. Pei, B. Chen, Y. Song, T. Zhang, W. Yang, and J. Shaman (2020). Substantial undocumented infection facilitates the rapid dissemination of novel coronavirus (SARS-CoV-2). *Science 368*(6490), 489–493. 2, 4, 5

Lipsitch, M., E. Tchetgen Tchetgen, and T. Cohen (2010). Negative controls: a tool for detecting confounding and bias in observational studies. *Epidemiology 21*(3), 383–388. 19

Ma, Y., Y. Zhao, J. Liu, X. He, B. Wang, S. Fu, J. Yan, J. Niu, J. Zhou, and B. Luo (2020). Effects of temperature variation and humidity on the death of COVID-19 in Wuhan, China. *Science of The Total Environment 724*, 138226. 18

Marshall, M. G., T. R. Gurr, and K. Jaggers (2019). Polity IV Project. 29

Mathieu, E., H. Ritchie, L. Rodés-Guirao, C. Appel, C. Giattino, J. Hasell, B. Macdonald, S. Dattani, D. Beltekian, E. Ortiz-Ospina, and M. Roser (2020). Coronavirus pandemic (COVID-19). 17, 29, 35

Nunn, N. and D. Puga (2012). Ruggedness: The blessing of bad geography in Africa. *Review of Economics and Statistics 94*(1), 20–36. 18

Oster, E. (2012). Routes of infection: Exports and HIV incidence in Sub-saharan Africa. *Journal of the European Economic Association 10*(5), 1025–1058. 5

Page, K. R., M. Venkataramani, C. Beyrer, and S. Polk (2020). Undocumented U.S. immigrants and Covid-19. *New England Journal of Medicine 382*(21), e62. 2, 4

Parker, P. M. (1997). *National Cultures of the World: A Statistical Reference, Cross-Cultural Statistical Encyclopedia of the World* (4th ed.). Westport, CT: Greenwood Press. 29, 33, 37

Rojanaworarit, C. and S. El Bouzaidi (2021). International labour trafficking: A neglected social origin of COVID-19. *The Lancet Regional Health – Western Pacific 8*, 100121. doi: 10.1016/j.lanwpc.2021.100121. 2, 3, 4, 10, 21, 24, 25

Rojanaworarit, C. and S. El Bouzaidi (2022). Building a resilient public health system for international migrant workers: A case study and policy brief for COVID-19 and beyond. *Journal of Health Research 36*(5), 898–907. 2, 4, 5, 21

Shi, Q., D. Dorling, G. Cao, and T. Liu (2020). Changes in population movement make COVID-19 spread differently from SARS. *Social Science & Medicine 255*, 113036. 2

Slack, J. and H. Campbell (2016). On narco-coyotaje: Illicit regimes and their impacts on the US–Mexico border. *Antipode 48*(5), 1380–1399. 3

St John, R. K., A. King, D. de Jong, M. Bodie-Collins, S. G. Squires, and T. W. S. Tam (2005). Border screening for SARS. *Emerging infectious diseases 11*(1), 6–10. 2, 5

Stankov, P. (2024). Will voters polarize over pandemic restrictions? theory and evidence from COVID-19. *Economic Modelling 136*, 106749. 2

Todres, J. and A. Diaz (2021). COVID-19 and Human Trafficking—the Amplified Impact on Vulnerable Populations. *JAMA Pediatrics 175*(2), 123–124. 2, 4, 5, 21, 25

UNHCR [United Nations High Commissioner for Refugees] (2019). Population Statistics. Report, UNHCR, Vienna: UNODC. 29, 34

UNODC [United Nations Office on Drugs and Crimes] (2011). The Role of Organized Crime in the Smuggling of Migrants from West Africa to the European Union. Report, UNODC, Vienna: UNODC. 3, 18, 19

UNODC [United Nations Office on Drugs and Crimes] (2014). Global Report on Trafficking in Persons. Report, UNODC, Vienna: UNODC. 9

UNODC [United Nations Office on Drugs and Crimes] (2016). Global Report on Trafficking in Persons. Report, UNODC, Vienna: UNODC. 3, 9

UNODC [United Nations Office on Drugs and Crimes] (2018). Global Study on Smuggling of Migrants. Report, UNODC, Vienna: UNODC. 3, 12

UNODC [United Nations Office on Drugs and Crimes] (2020). Individual Drug Seizure Cases (IDS). Report, UNODC, DATAUNODC. 19, 29, 38

U.S. Department of State (2001). Trafficking in Persons Report. Report, U.S. Department of State, Washington, D.C. 2, 8, 9

U.S. Department of State (2005). Trafficking in Persons Report. Report, U.S. Department of State, Washington, D.C. 9

U.S. Department of State (2009). Trafficking in Persons Report. Report, U.S. Department of State, Washington, D.C. 30

U.S. Department of State (2017). Trafficking in Persons Report. Report, U.S. Department of State, Washington, D.C. 12

U.S. Department of State (2018). Trafficking in Persons Report. Report, U.S. Department of State, Washington, D.C. 9, 12

U.S. Department of State (2019). Trafficking in Persons Report. Report, U.S. Department of State, Washington, D.C. 3, 9, 11, 12

Wang, J., K. Tang, K. Feng, X. Lin, W. Lv, K. Chen, and F. Wang (2021). Impact of temperature and relative humidity on the transmission of COVID-19: a modelling study in China and the United States. *BMJ Open 11*(2), e043863. 18

Wang, M., A. Jiang, L. Gong, L. Luo, W. Guo, C. Li, J. Zheng, C. Li, B. Yang, J. Zeng, Y. Chen, K. Zheng, and H. Li (2020). Temperature Significant Change COVID-19 Transmission in 429 Cities. 18

Williams, H. A., R. L. Dunville, S. I. Gerber, D. D. Erdman, N. Pesik, D. Kuhar, K. A. Mason, L. Haynes, L. Rotz, J. St Pierre, et al. (2015). CDC's early response to a novel viral disease, Middle East Respiratory Syndrome Coronavirus (MERS-CoV), September 2012-May 2014. *Public Health Reports 130*(4), 307–317. PMC4547580. 2, 5

Worsnop, C. Z. (2019). The Disease Outbreak-Human Trafficking Connection: A Missed Opportunity. *Health Security 17*(3), 181–192. 2

Appendix A. Data and Data Sources

Table A1
Data sources and description

Variable	Source and Description
Relative TIP inflow; TIP standards & amnesty	Human Trafficking Indicators, 2000–11: A New Dataset Frank (2013). Relative risk of TIP (trafficking in persons) inflow Difference of (i) destination indicator, averaged 2000–11, and (ii) source indicator, averaged 2000–11.
Confirmed pandemic numbers	H1N1 sample: `https://en.wikipedia.org/wiki/2009_swine_flu_pandemic_tables` COVID-19 sample: `https://github.com/CSSEGISandData/COVID-19`
Coastline distance (km) and land area (km^2)	The World Factbook.
Gravity-measures: Contiguity, Common language, PTA, Distance, 13 region dummies, island & landlocked dummy	The Dynamic Gravity Dataset Gurevich and Herman (2018). H1N1 sample: 2009 COVID-19 sample: 2016 (latest available) *Distance* is the population-weighted average of city-to-city bilateral distances in kilometers between each major city.
Polity measure of democracy and Constraint on Executive	Polity IV (Marshall et al., 2019). H1N1 sample: 2000–08 COVID-19 sample: 2010–18
Refugee and asylum-seeker flows	UNHCR [United Nations High Commissioner for Refugees] (2019) Population Statistics. H1N1 sample: 2009 COVID-19 sample: 2018 (latest available) Historical flows ratio are averaged for 1990–2005. In the data, bilateral-annual values between 1 to 4 are coded as "*" to protect the anonymity of individuals, in these cases, I impute * as 1.
Cocaine seizures, cocaine and amphetamine inflow	UNODC [United Nations Office on Drugs and Crimes] (2020). Cocaine national seizures summed at country level (2012–16). Cocaine and ATS (amphetamine-type stimulants) summed at destination country (2011–16) from the Individual Drug Seizures reports.
Economic and health variables	World Development Indicators. H1N1 sample: 2000–08 COVID-19 sample: 2010–18 Log GDP per capita is real GDP per capita (USD millions, constant2011); log government health expenditure per capita and log health expenditure per capita are both PPP, current international dollars); old age dependency is the ratio of above 64 to working -aged population (above 15 to 64); log population density is log of population divided by land area; log refugee stock and log migrant stock are the log of refugee population and log of international migrant stock. The World Bank data does not include Anguilla and Taiwan, so for these two cases I use the gravity data source Gurevich and Herman (2018).
Migration flows	Bilateral international migration flow estimates for 200 countries Abel and Cohen (2019). H1N1 sample: 2005–10 5–year estimates COVID-19 sample: 2010–15 5–year estimates (latest available) The migration flow estimates are the Demographic Accounting Pseudo Bayesian Closed estimates, aggregated up to destination countries. Migration inflow from pandemic source country is aggregated up to destination countries with only the pandemic source countries as inflow source.
Geography variables (temperature, humidity, soil quality, land territory 100km to coast)	Parker (1997); Acemoglu et al. (2001). Temperature variables: mean temperature, minimum monthly low, minimum monthly high, maximum monthly low, maximum monthly high. Humidity variables: morning minimum, morning maximum, afternoon minimum, afternoon maximum. Soil quality (as a proxy of climate): low-latitude steppe, mid-latitude steppe, low-latitude desert, mid-latitude desert, dry steppe wasteland, and desert dry winter.
% Protestant, Muslim, and Roman Catholic; Ethno-linguistic fragmentation	Easterly and Levine (1997); La Porta et al. (1999). Religion proportion for three most wide-spread religions in the world. Most recent of 1980–1995. Ethno-linguistic fragmentation is the average value of five different indices fractionalization of ethonolinguistic fractionalization, range 0 to 1, increasing in fragmentation. The five component indices are: (1) index of ethnolinguistic fractionalization in 1960, which measures the probability that two randomly selected people from a given country will not belong to the same ethnolinguistic group (the index is based on the number and size of population groups as distinguished by their ethnic and linguistic status); (2) probability of two randomly selected individuals speaking different languages; (3) probability of two randomly selected individuals do not speak the same language; (4) percent of the population not speaking the official language; and (5) percent of the population not speaking the most widely used language.
Mass mobilization and protest (H1N1 sample only)	Mass Mobilization Data Project, 1990–2018. Clark and Regan (2016). I filter the data to the period April–July 2009, then aggregate up the *number of participants* estimates at the country level. If this number is positive for a country in this period, the dummy is coded as 1, and 0 otherwise.
Number of tests conducted (COVID-19 sample only)	Mathieu et al. (2020) Daily recorded number of tests for countries are sporadic at the first few weeks. For each country, I use the latest available (cumulative) recorded test numbers for the day, by the end of April 2020.

Trafficking indicators

The destination and source indicators from Frank (2013) are constructed as follows. For each country-year, there is a destination, source, plus transit indicator going from 1 to 3 depending on the order in which a country's profile mentions *destination*, *source*, or *transit*. Returning to the Switzerland 2009 example, the profile begins by stating that the country is "primarily a destination and, to a lesser extent, a transit country for women and children trafficked for the purposes of commercial sexual exploitation and forced labor" (U.S. Department of State 2009). So the destination indicator is recorded as three since *destination* is mentioned first, and the transit indicator is recorded as two since *transit* is mentioned second. The source indicator is recorded as 0 since it was never mentioned; if the source indicator had been mentioned and mentioned last, the source indicator would be 1.

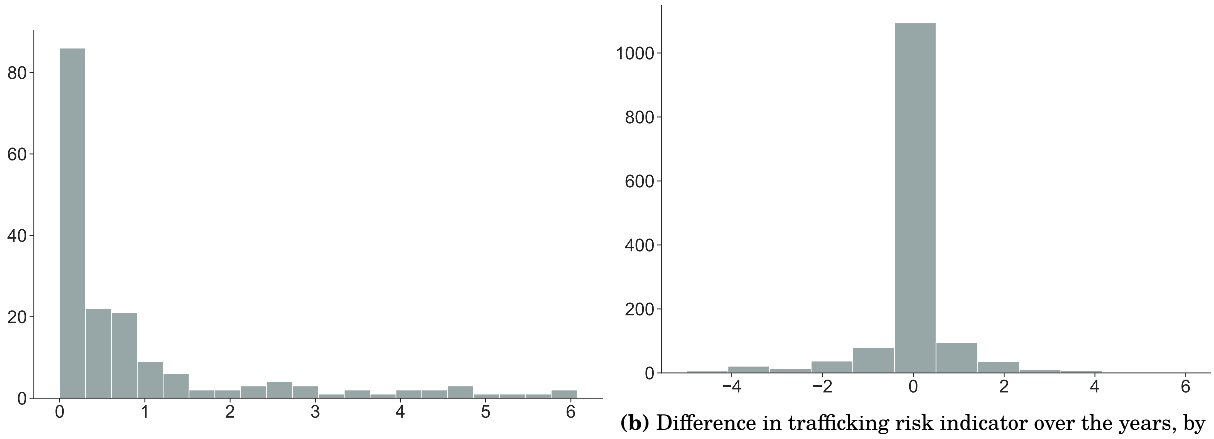

(a) Variance of trafficking risk indicator, by country

(b) Difference in trafficking risk indicator over the years, by country-year

Fig. A1. Variation in the trafficking risk (relative TIP inflow) indicator. (a) Variance of the trafficking measure over time for individual countries. (b) Year-on-year change in the trafficking risk measure for the country-year observations.

Table A2
List of country codes and region

Region	ISO-3	Country	2001–11 Relative TIP inflow	Region	ISO-3	Country	2001–11 Relative TIP inflow
Africa	AGO	Angola	-2.6	Europe	DEU	Germany	1
Africa	BDI	Burundi	-2.8	Europe	DNK	Denmark	2.4
Africa	BEN	Benin	-2.1	Europe	ESP	Spain	2.6
Africa	BFA	Burkina Faso	-2	Europe	EST	Estonia	-2.4
Africa	BWA	Botswana	-1.3	Europe	FIN	Finland	2.3
Africa	CAF	Central African Republic	-1.5	Europe	FRA	France	2.9
Africa	CIV	Cote d'Ivoire	2	Europe	GBR	United Kingdom	2.7
Africa	CMR	Cameroon	-2	Europe	GEO	Georgia	-2.8
Africa	COD	Congo (Kinshasa)	-2.2	Europe	GRC	Greece	2.2
Africa	COG	Congo (Brazzaville)	0	Europe	HRV	Croatia	-0.4
Africa	COM	Comoros	-3	Europe	HUN	Hungary	-1.2
Africa	DJI	Djibouti	-1.1	Europe	IRL	Ireland	2.5
Africa	DZA	Algeria	1.6	Europe	ISL	Iceland	3
Africa	EGY	Egypt	-1.3	Europe	ITA	Italy	2.9
Africa	ERI	Eritrea	-3	Europe	LTU	Lithuania	-2.1
Africa	ETH	Ethiopia	-3	Europe	LUX	Luxembourg	2.6
Africa	GAB	Gabon	3	Europe	LVA	Latvia	-2.6
Africa	GHA	Ghana	-2	Europe	MDA	Moldova	-2.7
Africa	GIN	Guinea	-2	Europe	MKD	Macedonia	0.1
Africa	GMB	Gambia	-2	Europe	MLT	Malta	2.1
Africa	GNB	Guinea-Bissau	-3	Europe	MNE	Montenegro	-0.2
Africa	GNQ	Equatorial Guinea	2.7	Europe	NLD	Netherlands	0.8
Africa	KEN	Kenya	-2	Europe	NOR	Norway	2.8
Africa	LBR	Liberia	-1.4	Europe	POL	Poland	-1.9
Africa	LBY	Libya	2.1	Europe	PRT	Portugal	2.7
Africa	MAR	Morocco	-2.2	Europe	ROU	Romania	-2.5
Africa	MDG	Madagascar	-3	Europe	SRB	Serbia	-2
Africa	MLI	Mali	-1.9	Europe	SVK	Slovakia	-2.2
Africa	MRT	Mauritania	-0.9	Europe	SVN	Slovenia	0
Africa	MUS	Mauritius	-2.6	Europe	SWE	Sweden	2.8
Africa	MWI	Malawi	-2.3	Europe	UKR	Ukraine	-2.5
Africa	NER	Niger	-2.1	Middle East	AFG	Afghanistan	-2.5
Africa	NGA	Nigeria	-2	Middle East	ARE	United Arab Emirates	3
Africa	RWA	Rwanda	-2.6	Middle East	BHR	Bahrain	3
Africa	SDN	Sudan	-0.9	Middle East	IRN	Iran	-2.2
Africa	SEN	Senegal	-2.1	Middle East	IRQ	Iraq	-1.3
Africa	SLE	Sierra Leone	-2.2	Middle East	ISR	Israel	2.6
Africa	SOM	Somalia	-2	Middle East	JOR	Jordan	2.6
Africa	SYC	Seychelles	-1	Middle East	KWT	Kuwait	2.9
Africa	TCD	Chad	-1.9	Middle East	LBN	Lebanon	2.3
Africa	TGO	Togo	-1.7	Middle East	OMN	Oman	3
Africa	TUN	Tunisia	-1.1	Middle East	QAT	Qatar	2.8
Africa	TZA	Tanzania	-1.8	Middle East	SAU	Saudi Arabia	3
Africa	UGA	Uganda	-2	Middle East	SYR	Syria	3
Africa	ZAF	South Africa	-0.5	Middle East	YEM	Yemen	-1.4
Africa	ZMB	Zambia	-2.3	North America	CAN	Canada	0.5
Africa	ZWE	Zimbabwe	-2.3	North America	MEX	Mexico	-1.9
Caribbean	ATG	Antigua and Barbuda	3	North America	USA	US	1.4
Caribbean	BHS	Bahamas	2.7	Pacific	AUS	Australia	2.3
Caribbean	BRB	Barbados	0.4	Pacific	FJI	Fiji	-1
Caribbean	CUB	Cuba	-1.7	Pacific	FSM	Federated States of Micronesia	-1.7
Caribbean	DOM	Dominican Republic	-2	Pacific	KIR	Kiribati	-3
Caribbean	HTI	Haiti	-2.2	Pacific	NZL	New Zealand	1
Caribbean	JAM	Jamaica	-1.6	Pacific	PLW	Palau	2.5
Caribbean	LCA	Saint Lucia	3	Pacific	PNG	Papua New Guinea	0.6
Caribbean	TTO	Trinidad and Tobago	1.7	Pacific	SLB	Solomon Islands	3
Caribbean	VCT	Saint Vincent and the Grenadines	-1.3	Pacific	TON	Tonga	-1
Central America	BLZ	Belize	-0.4	South America	ARG	Argentina	-0.9
Central America	CRI	Costa Rica	-0.5	South America	BOL	Bolivia	-3
Central America	GTM	Guatemala	-2	South America	BRA	Brazil	-1.5
Central America	HND	Honduras	-2.6	South America	CHL	Chile	-1.9
Central America	NIC	Nicaragua	-2.7	South America	COL	Colombia	-2.5
Central America	PAN	Panama	-1.5	South America	ECU	Ecuador	-2
Central America	SLV	El Salvador	-2	South America	GUY	Guyana	-2
Central Asia	KGZ	Kyrgyzstan	-2.1	South America	PER	Peru	-2.6
Central Asia	TJK	Tajikistan	-3	South America	PRY	Paraguay	-1.9
Central Asia	UZB	Uzbekistan	-3	South America	SUR	Suriname	1.7
East Asia	CHN	China	-1.9	South America	URY	Uruguay	-2.7
East Asia	JPN	Japan	2.4	South America	VEN	Venezuela	-1.6
East Asia	KOR	Korea, South	-1.8	South Asia	BGD	Bangladesh	-3
East Asia	MNG	Mongolia	-2.3	South Asia	IND	India	-1.5
East Asia	TWN	Taiwan	1	South Asia	LKA	Sri Lanka	-1
Eurasia	KAZ	Kazakhstan	-1.6	South Asia	MDV	Maldives	3
Eurasia	RUS	Russia	-2.1	South Asia	NPL	Nepal	-3
Eurasia	TUR	Turkey	2.5	South Asia	PAK	Pakistan	-1.7
Europe	ALB	Albania	-3	Southeast Asia	BRN	Brunei	2.5
Europe	ARM	Armenia	-1.9	Southeast Asia	IDN	Indonesia	-2.1
Europe	AUT	Austria	2.3	Southeast Asia	KHM	Cambodia	-1.4
Europe	AZE	Azerbaijan	-2.6	Southeast Asia	LAO	Laos	-2.2
Europe	BEL	Belgium	2.2	Southeast Asia	MMR	Myanmar	-2.5
Europe	BGR	Bulgaria	-1.9	Southeast Asia	MYS	Malaysia	0.6
Europe	BIH	Bosnia and Herzegovina	0	Southeast Asia	PHL	Philippines	-1.9
Europe	BLR	Belarus	-2.5	Southeast Asia	SGP	Singapore	3
Europe	CHE	Switzerland	3	Southeast Asia	THA	Thailand	-1.5
Europe	CYP	Cyprus	3	Southeast Asia	TLS	Timor-Leste	2.8
Europe	CZE	Czechia	-1.7	Southeast Asia	VNM	Vietnam	-1.6

Appendix B. OLS

Fig. B1. OLS relationship: Trafficking risk and the H1N1 pandemic. Log confirmed cases per million population as of June 2009 and trafficking risk. The graph "soft-censors" the top five percent of confirmed cases.

Table B1
Trafficking risk and confirmed cases: OLS estimates

	Dep. var. is log confirmed cases per population							
	Full Sample						H1N1 Sample	COVID-19 Sample
	(1)	(2)	(3)	(4)	(5)	(6)	(7)	(8)
Relative TIP flow	0.54***	0.46***	0.46***	0.43***	0.43***	0.46***	0.46***	0.41***
	(0.06)	(0.06)	(0.06)	(0.07)	(0.08)	(0.06)	(0.07)	(0.08)
Covid-19 dummy	4.01***	4.38***	4.03***	4.45***	4.57***	4.45***		
	(0.27)	(0.24)	(0.28)	(0.39)	(0.31)	(0.34)		
Contiguity dummy			–1.13*	–1.10**	–0.92*	–1.42***	–0.97*	–2.15***
			(0.61)	(0.53)	(0.55)	(0.52)	(0.56)	(0.74)
Common lang. dummy			0.93*	1.00	0.96	0.51	0.27	1.92*
			(0.53)	(0.70)	(0.72)	(0.56)	(0.43)	(1.01)
Distance from Gzero			–0.08**	–0.09*	–0.08**	–0.12***	0.15	–0.07
			(0.03)	(0.04)	(0.04)	(0.04)	(0.11)	(0.13)
PTA dummy			–0.90***	–0.43	–0.37	–0.45	–0.85**	1.82***
			(0.32)	(0.45)	(0.37)	(0.48)	(0.37)	(0.47)
Region dummies		Yes	Yes	Yes	Yes	Yes	Yes	Yes
F-test: Regions=0		15.5***	13.44***	17.24***	17.59***	15.16***	20.26***	24.22***
F-test: Gravity=0			4.57**	2.74**	2.95**	3.63**	2.29*	9.13***
R^2	0.47	0.66	0.68	0.67	0.72	0.70	0.57	0.65
Weighted by				Cases	Deaths	Fatality		
Countries	174	174	174	174	174	174	135	168
Observations	303	303	303	303	303	302	135	168

Notes—The dependent variable is the log of confirmed cases per million population as of the third month of each pandemic (June 2009 for the H1N1 pandemic and March 2020 for the COVID-19 pandemic). The relative TIP flow measure is the ratio of whether a country is reported as mainly a destination or source in international trafficking in persons (TIP) defined in Eq. (1). The gravity-type controls to the pandemic source country (Gurevich and Herman 2018) are for the years 2008 and 2016 (latest available) for the H1N1 and COVID-19 pandemic, respectively. Columns (4)–(6) are weighted-least squares regressions where observations are weighted by log confirmed cases, log deaths, and the (inverse) log case fatality rate, respectively. Robust standard errors in parentheses. *** $p < 0.01$, ** $p < 0.05$, * $p < 0.1$.

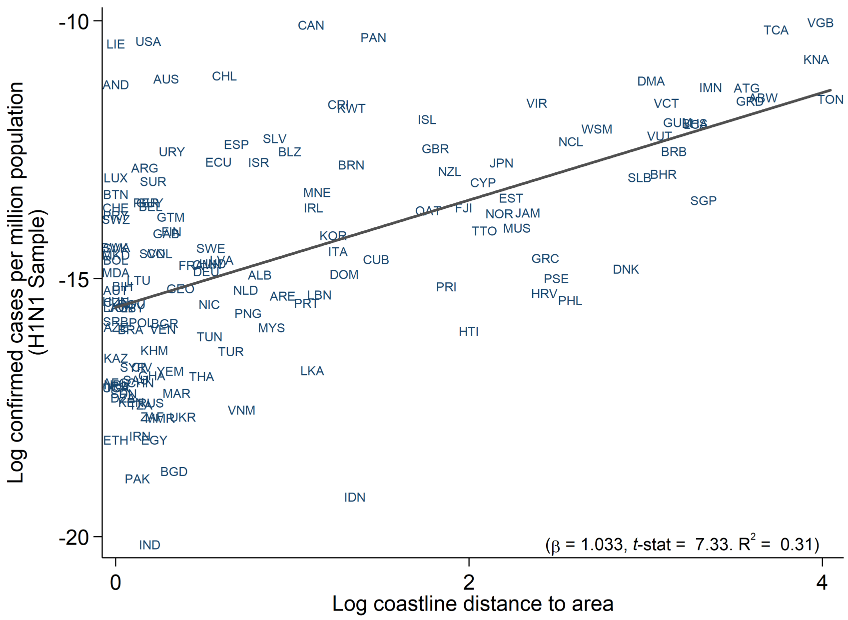

Fig. B2. Reduced form relationship: Trafficking risk and the H1N1 pandemic. Log confirmed cases per million population as of June 2009 and the log coastline length to area. The graph "soft-censors" the top five percent of confirmed cases.

Appendix C. Robustness: Additional Controls

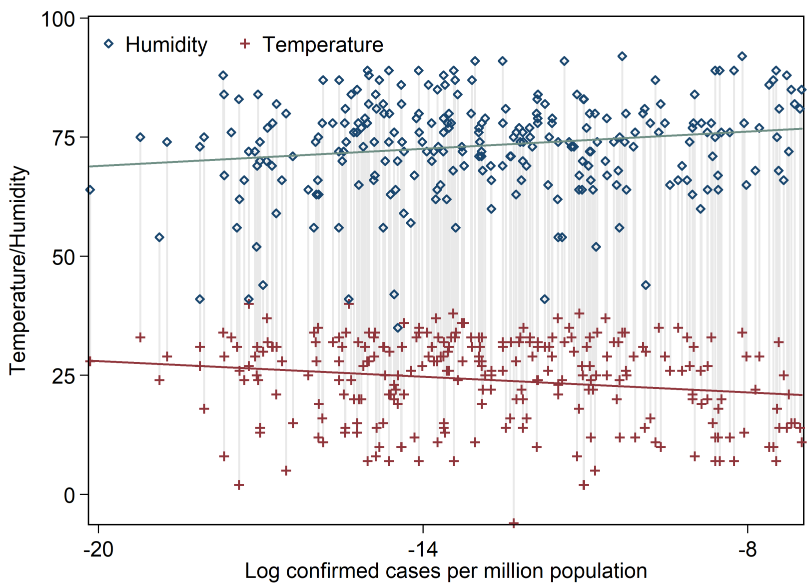

Fig. C1. Temperature and humidity effects on confirmed cases. Scatterplot and linear fit of temperature and humidity on the log confirmed cases per million population as of the 3rd month into the H1N1 pandemic (June 2009 for H1N1 and March 2020 for COVID-19). Temperature is the minimum monthly high (degree Celsius), and (relative) humidity is the afternoon maximum; both measures are taken directly from Acemoglu et al. (2001), originally from Parker (1997). Please see Table C4.

Table C1
International movements factors

	(1)	(2)	(3)	(4)	(5)	(6)	(7)	(8)	(9)
				A. Two-Stage Least Squares					
Relative TIP flow	1.40***	1.17***	1.20***	0.95***	1.06***	1.04***	1.39***	1.15***	0.76***
	(0.31)	(0.21)	(0.19)	(0.16)	(0.22)	(0.21)	(0.27)	(0.20)	(0.15)
Log migration inflow from pandemic source	–0.19**								0.01
	(0.08)								(0.05)
Log migration inflow									
Log of migrant stock			–0.31***						0.07
			(0.11)						(0.14)
Log of asylum-seekers inflow				–0.19***					–0.06
				(0.06)					(0.08)
Log of refugee seekers inflow					–0.15***				0.09
					(0.05)				(0.18)
Log refugee stock						–0.12**			–0.19
						(0.05)			(0.16)
Log tourist arrivals							–0.22*		–0.09
							(0.12)		(0.10)
Log tourism receipts as % of total exports								0.38***	0.26**
								(0.13)	(0.12)
First-stage F-stat	21.88	38.77	49.43	53.38	19.79	21.11	31.34	39.66	40.12
				B. First Stage for *relative TIP inflow*					
Log coastline to area	0.62***	0.79***	0.80***	0.88***	0.75***	0.80***	0.64***	0.77***	0.86***
	(0.13)	(0.13)	(0.11)	(0.12)	(0.17)	(0.17)	(0.11)	(0.12)	(0.14)
First-stage F-stat									
				C. Ordinary Least Squares					
Relative TIP flow	0.42***	0.43***	0.45***	0.46***	0.43***	0.41***	0.45***	0.46***	0.45***
	(0.05)	(0.05)	(0.05)	(0.06)	(0.05)	(0.05)	(0.06)	(0.05)	(0.06)
Region dummies	Yes	Yes	Yes	Yes	Yes	Yes	Yes	Yes	Yes
Gravity controls	Yes	Yes	Yes	Yes	Yes	Yes	Yes	Yes	Yes
Countries	172	172	173	150	265	162	168	164	138
Observations	300	300	300	257	265	279	291	288	235

Notes—Panel A reports the two-stage least-squares results where the dependent variable is the log of confirmed cases per million population as of 3rd month into the pandemic. Panel B reports the corresponding first stages. Panel C reports the analogous OLS estimates. All panels include the same covariates but are not always reported in Panels B and C to conserve space. Specifications follow column (4) of Table 1, with the below-stated additional controls. Column (1) includes the log of migration inflow from the source country of the pandemic (Mexico for H1N1 and China for COVID-19), averaged over 2005–10 and 2010–15, respectively. Column (2) includes log of total migration inflow. All migration flow data come from the dyadic estimates data (Abel and Cohen 2019), averaged over 2005–10 and 2010–15 for the H1N1 and COVID-19 pandemic, respectively. Columns (3) and (6) include the log of migrant and refugee stock. Columns (4) and (5) include the log of asylum-seekers and refugee inflow, with the data taken directly from the UNHCR [United Nations High Commissioner for Refugees] (2019), for the years 2009 and 2018 for the H1N1 and COVID-19 pandemic, respectively. Columns (7) and (8) include the log of international tourist arrivals and the receipts as a % of total exports. Unless otherwise stated, all variables come from the World Development Indicators, averaged over the years 2000–08 and 2010–18 for the H1N1 and COVID-19 pandemic, respectively. Robust standard errors in parentheses. *** $p < 0.01$, ** $p < 0.05$, * $p < 0.1$.

Table C2

Institutional and Health Factors

	(1)	(2)	(3)	(4)	(5)	(6)	(7)	(8)	(9)
					A. Two-Stage Least Squares				
Relative TIP flow	1.54***	1.10***	2.47**	1.77**	0.61***	1.43***	2.01**	2.74*	1.48***
	(0.28)	(0.25)	(1.22)	(0.77)	(0.15)	(0.33)	(0.85)	(1.64)	(0.30)
Anti-TIP standards	–1.80**								
	(0.82)								
TIP victims amnesty	–3.11***								
	(1.00)								
Polity measure of democracy		0.02							
		(0.09)							
Constraint on executive		0.08							
		(0.28)							
Log GDP per capita			–2.38						
			(1.73)						
% Government expenditure of GDP				0.01					
				(0.05)					
Log govt. health expenditure per capita				–0.91					
				(0.76)					
Log conducted tests (COVID-19only)					–0.04				
					(0.13)				
(Old) Age dependency						–0.02			
						(0.05)			
Log infant mortality							1.63		
							(1.38)		
Log health expenditure per capita								–2.54	
								(2.28)	
First-stage F-stat	32.35	20.63	4.48	6.00	25.30	17.89	5.69	2.99	24.21
					B. First Stage for *relative TIP inflow*				
Log coastline to area	0.60***	0.78***	0.24**	0.31**	1.01***	1.01***	0.57***	0.29**	0.62***
	(0.11)	(0.17)	(0.11)	(0.13)	(0.20)	(0.20)	(0.13)	(0.12)	(0.13)
					C. Ordinary Least Squares				
Relative TIP flow	0.45***	0.41***	0.14**	0.16***	0.48***	0.38***	0.18***	0.07	0.46***
	(0.06)	(0.06)	(0.06)	(0.06)	(0.09)	(0.05)	(0.06)	(0.06)	(0.06)
Region dummies	Yes	Yes	Yes	Yes	Yes	Yes	Yes	Yes	Yes
Gravity controls	Yes	Yes	Yes	Yes	Yes	Yes	Yes	Yes	Yes
Countries	174	154	170	164	81	172	173	170	174
Observations	303	267	296	279	156	300	301	296	303

Notes—Panel A reports the two-stage least-squares results where the dependent variable is the log of confirmed cases per million population as of 3rd month into the pandemic. Panel B reports the corresponding first stages. Panel C reports the analogous OLS estimates. All panels include the same covariates but are not always reported in Panels B and C to conserve space. Specifications follow column (4) of Table 1, with the below-stated additional controls. Column (1) includes the trafficking-specific institutions measure for compliance with the minimum standards for TIP elimination and protection services for victims. Column (2) includes the average constraint on the executive measure (2000-08 and then 2010–18 for the two pandemics) from the Polity data. Column (3) includes the log GDP per capita. Column (4) includes other measures of government size, including the size of government expenditure in relation to GDP, government health expenditure, and the *reported* numbers of tests conducted during the COVID-19 pandemic (Mathieu et al. 2020). Column (5) includes the ratio of above-64 to working-age population. Column (6) includes the log of infant mortality rate. Column (7) includes total health expenditure per capita. Column (8) includes all the controls except for log conducted tests. Unless otherwise stated, all variables come from the World Development Indicators, averaged over the years 2000–08 and 2010–18 for the H1N1 and COVID-19 pandemic, respectively. Robust standard errors in parentheses. *** $p < 0.01$, ** $p < 0.05$, * $p < 0.1$.

Table C3
Social and Cultural Factors

	(1)	(2)	(3)	(4)	(5)	(6)	(7)	(8)	(9)
				A. Two-Stage Least Squares					
Relative TIP flow	1.28***	1.00***	1.78***	1.45***	1.46***	1.54***	1.65***	1.42***	0.53**
	(0.25)	(0.20)	(0.47)	(0.46)	(0.30)	(0.29)	(0.45)	(0.29)	(0.27)
Transfers/subsidies as % of government expenses	–0.00								–0.01
	(0.01)								(0.01)
% Roman Catholic, Protestant, and Muslim			0.02**						–0.00
			(0.01)						(0.00)
ELF				–0.07					0.77
				(0.73)					(0.65)
Mass mobilization and protest dummy					–0.29				
					(0.54)				
Log population density						–0.10			0.24
						(0.19)			(0.15)
% population in urban areas							–0.04		0.01
							(0.02)		(0.01)
Log total fisheries production								–0.01	–0.02
								(0.06)	(0.05)
First-stage F-stat	26.88	28.24	12.93	8.31	23.58	33.10	14.33	23.69	9.15
				B. First Stage for *relative TIP inflow*					
Log coastline to area	0.75***	0.71***	0.50***	0.50***	0.61***	0.71***	0.44***	0.44***	0.65***
	(0.14)	(0.13)	(0.14)	(0.17)	(0.13)	(0.12)	(0.12)	(0.12)	(0.22)
				C. Ordinary Least Squares					
Relative TIP flow	0.45***	0.36***	0.47***	0.48***	0.46***	0.45***	0.30***	0.43***	0.28***
	(0.05)	(0.07)	(0.06)	(0.07)	(0.05)	(0.05)	(0.06)	(0.05)	(0.10)
Region dummies	Yes	Yes	Yes	Yes	Yes	Yes	Yes	Yes	Yes
Gravity controls	Yes	Yes	Yes	Yes	Yes	Yes	Yes	Yes	Yes
Countries	136	148	166	122	303	174	173	173	84
Observations	229	231	291	213	303	303	301	301	134

Notes—Panel A reports the two-stage least-squares results where the dependent variable is the log of confirmed cases per million population as of 3rd month into the pandemic. Panel B reports the corresponding first stages. Panel C reports the analogous OLS estimates. All panels include the same covariates but are not always reported in Panels B and C to conserve space. Specifications follow column (4) of Table 1, with the below-stated additional controls. Column (1) includes the average of transfers and subsidies as a percentage of government expenses over the years 2000–08 and 2010–18 (for the H1N1 and COVID-19 pandemic, respectively). Column (2) includes the primary and secondary school net enrollment rate. Column (3) includes the percentage of the population belonging to the Roman Catholic, Muslim, and Protestant religions (La Porta et al. 1999). Column (4) includes the average of 5 ethnolinguistic fragmentation indices taken directly from (La Porta et al. (1999), originally from Easterly and Levine (1997)). Column (5) includes a dummy available only for the H1N1 sample, for whether there was mass mobilization or protest in the first four months (April–July) of the H1N1 pandemic, with the data aggregated up to the country level (Clark and Regan 2016). Non-observations are imputed as zero. Column (6) includes the log of population divided by land area. Column (7) includes the percentage of population living in urban areas. Column (8) includes the total volume (metric tons) of aquatic species caught for all commercial, industrial, recreational, and subsistence purposes. Column (9) includes all the variables except for the mass mobilization dummy. Unless otherwise stated, all variables come from the World Development Indicators, averaged over the years 2000–08 and 2010–18 for the H1N1 and COVID-19 pandemic, respectively. Robust standard errors in parentheses. *** $p < 0.01$, ** $p < 0.05$, * $p < 0.1$.

Table C4
Geography Factors

	(1)	(2)	(3)	(4)	(5)	(6)	(7)	(8)
	A. Two-Stage Least Squares							
Relative TIP flow	1.30***	1.54***	0.68***	1.46***	1.48***	1.64***	1.29***	0.79***
	(0.36)	(0.31)	(0.22)	(0.35)	(0.33)	(0.45)	(0.28)	(0.18)
Island dummy	0.98							–0.33
	(0.60)							(0.54)
Landlocked dummy	0.73							0.61
	(0.45)							(0.52)
Latitude		2.46						1.11
		(1.77)						(1.88)
Land territory 100km of sea coast			2.65***					3.24***
			(0.58)					(0.65)
Mean temperature				–0.11**				–0.38
				(0.05)				(0.28)
Temperature range variables					6.37			9.47*
[ρ-value]					[0.17]			[0.09]
Humidity range variables						10.03**		15.26**
[ρ-value]						[0.04]		[0.00]
Climate/soil quality variables							9.35	8.01
[ρ-value]							[0.15]	[0.24]
First-stage F-stat	11.27	23.64	24.66	14.80	17.08	11.28	20.50	22.33
	B. First Stage for *relative TIP inflow*							
Log coastline to area	0.52***	0.62***	1.51***	0.62***	0.64***	0.53***	0.69***	1.74***
	(0.15)	(0.13)	(0.30)	(0.16)	(0.15)	(0.16)	(0.15)	(0.37)
	C. Ordinary Least Squares							
Relative TIP flow	0.39***	0.47***	0.54***	0.49***	0.46***	0.48***	0.48***	0.54***
	(0.06)	(0.06)	(0.09)	(0.06)	(0.07)	(0.07)	(0.06)	(0.13)
Region dummies	Yes	Yes	Yes	Yes	Yes	Yes	Yes	Yes
Gravity controls	Yes	Yes	Yes	Yes	Yes	Yes	Yes	Yes
Countries	174	174	59	150	150	150	150	59
Observations	303	303	104	263	263	263	263	104

Notes—Panel A reports the two-stage least-squares results where the dependent variable is the log of confirmed cases per million population as of 3rd month into the pandemic. Panel B reports the corresponding first stages. Panel C reports the analogous OLS estimates. All panels include the same covariates but are not always reported in Panels B and C to conserve space. Specifications follow column (4) of Table 1, with the below-stated additional controls. Column (1) includes the dummies for whether a country is an island and is landlocked (Gurevich and Herman 2018). Column (2) includes (absolute) latitude. Column (3) includes the proportion of land territory within 100km of coastlines (Acemoglu et al. 2001). Column (4) includes mean temperature. Column (5) includes the four additional temperature variables: minimum monthly low, minimum monthly high, maximum monthly low, and maximum monthly high. Column (6) includes four humidity variables: morning minimum, morning maximum, afternoon minimum, and afternoon maximum. Column (7) includes six dummies for soil quality (as a proxy of climate): low-latitude steppe, mid-latitude steppe, low-latitude desert, mid-latitude desert, dry steppe wasteland, and desert dry winter. Column (8) includes all the variables together. Columns (5)–(8) report the joint test of significance χ^2 and ρ-value for the temperature, humidity, and soil quality variables. All temperature, humidity, and climate/soil data come directly from Acemoglu et al. (2001), originally from Parker (1997). ρ-value for the joint test of significance in brackets. Robust standard errors in parentheses. *** p < 0.01, ** p < 0.05, * p < 0.1.

Appendix D. Robustness: Over-Identification Tests

Table D1
Overidentification Tests

	(1)	(2)	(3)	(4)	(5)	(6)
	A. Two-Stage Least Squares					
Relative TIP flow	1.07***	1.06***	1.20***	1.31***	1.70***	1.58***
	(0.28)	(0.22)	(0.30)	(0.23)	(0.39)	(0.29)
First-stage F-stat	85.80	61.11	51.99	36.13	31.77	21.25
Hansen test		.01		.57		.33
	B. First Stage for *relative TIP inflow*					
Log cocaine seizures per capita	0.36***	0.31***				
	(0.04)	(0.04)				
Log cocaine inflow per capita			0.32***	0.27***		
			(0.04)	(0.04)		
Log amphetamine inflow per capita					0.32***	0.22***
					(0.06)	(0.06)
Log coastline to area		0.64***		0.49***		0.42***
		(0.14)		(0.13)		(0.14)
	C. Log coastline to land area as exogenous variable					
Relative TIP flow		1.07***		1.15***		1.90***
		(0.32)		(0.35)		(0.72)
Log coastline to area		–0.02		0.20		–0.27
		(0.30)		(0.25)		(0.50)
Region dummies	Yes	Yes	Yes	Yes	Yes	Yes
Gravity controls	Yes	Yes	Yes	Yes	Yes	Yes
Countries	132	132	174	174	174	174
Observations	244	244	303	303	303	303

Notes—Panel A reports the two-stage least-squares results. The dependent variable is the log of confirmed cases per million population as of the 3rd month into the pandemic. Panel B reports the corresponding first stages. Panel C reports the second stage results with the alternative instruments as the only instrument for *relative TIP flow*, and with log coastline distance to land area entered as an exogenous in the second stage. Specifications follow column (4) of Table 1, with the below-stated additional controls. All panels include the same covariates but are not reported in Panels B and C to conserve space. Cocaine seizure (2012–16) and the drugs inflow data (2006–11) are from UNODC [United Nations Office on Drugs and Crimes] (2020). Robust standard errors in parentheses. *** $p < 0.01$, ** $p < 0.05$, * $p < 0.1$.

Appendix E. Robustness: Additional Tests

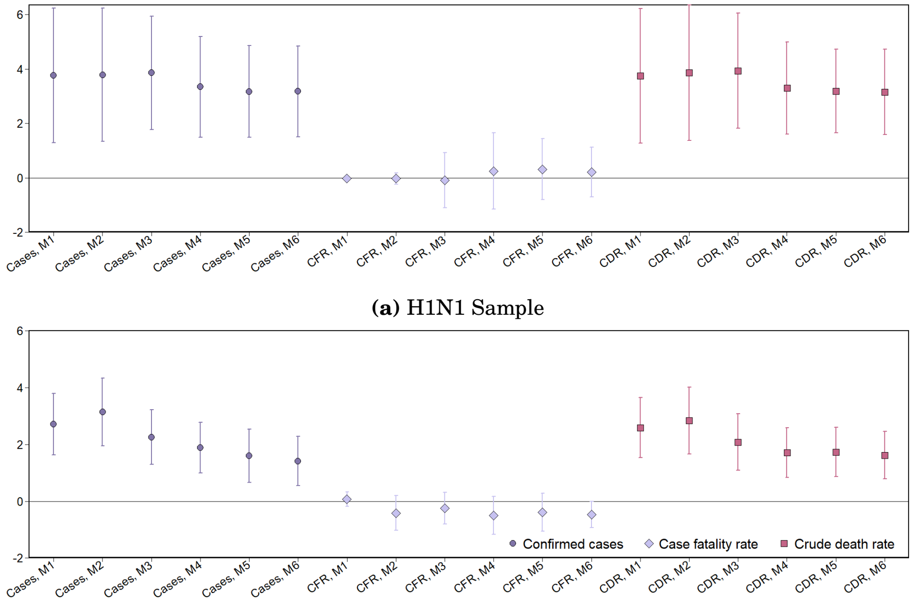

(**a**) H1N1 Sample

(**b**) COVID-19 Sample

Fig. E1. 2SLS Estimates by Month (Destination Indicator)

Notes—This figure replicates Fig. 6, with the mean of destination indicator as the estimand in the structural equation (2) instead of the measure defined in Eq. (1). The coefficient plot of two-stage least-squares estimates with the dependent variable as cumulative confirmed numbers from the 1st to 6th month of the pandemic and by the H1N1 and COVID-19 pandemic subsamples. The specification follows column (4) of Table 1. The vertical bars indicate the 95%

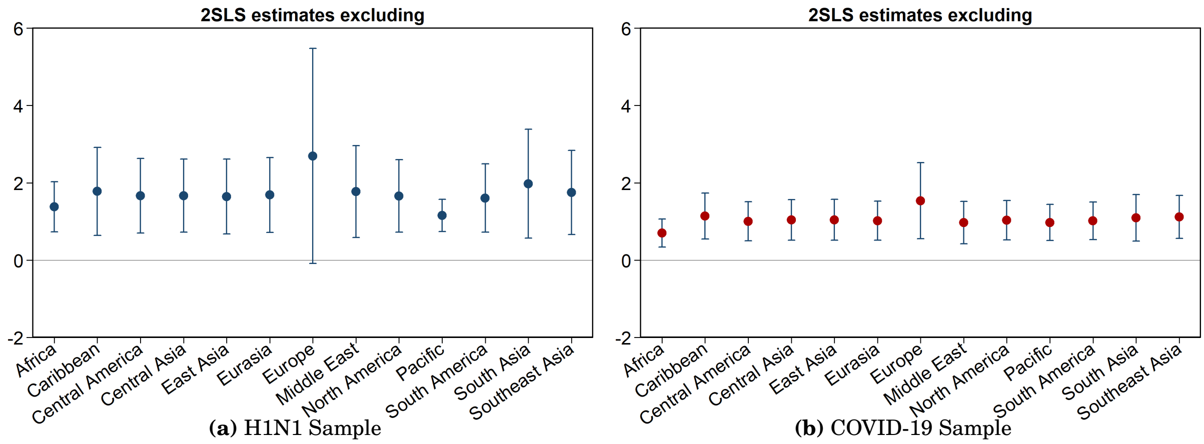

(**a**) H1N1 Sample (**b**) COVID-19 Sample

Fig. E2. Regional Jackknife. The plot of the 2SLS estimate of the trafficking risk (relative TIP inflow) measure on log confirmed cases (per million population) by the 3rd month into the pandemics, separately for the H1N1 and the COVID-19. Each column omits countries from one of the thirteen regions in turn. The specification otherwise follows column (4) of Table 1. The capped vertical bars indicate 95% confidence intervals.

Appendix F. SIRD: Proportional Increase in Contact Rate

Here, I model the relative risk of trafficking as augmenting the contact rate proportionally in the SIRD (Susceptible-Infectious-Recovered-Deceased) model. The objective is to derive a tractable specification from the SIRD model that allows trafficking to predict disease spread as a test of a specific mechanism. Specifically, I model trafficking as augmenting the contact rate. With simplifying assumptions for tractability, the augmented SIRD model reduces into Eq. (F.10), with τ capturing the association between trafficking and disease spread (Allcott et al. 2024). This model allows us to test whether trafficking augmenting the contact rate is a specific mechanism to the extent that τ is statistically positive.

Eq. (F.1) defines the population into four compartments: S_t, I_t, R_t, and D_t for the number of people who susceptible, infected, recovered, and deceased at a given time t, which is by weeks in this context. Eqs. (F.2) to (F.5) define the dynamics over time, where β_t is the contact rate (or rate of infection), γ is the rate of recovery, μ is the true risk of mortality (different from the CFR).

$$S_t + I_t + R_t + D_t = N \tag{F.1}$$

$$S_{t+1} - S_t = -\beta_t S_t \frac{I_t}{N} \tag{F.2}$$

$$I_{t+1} - I_t = \beta_t S_t \frac{I_t}{N} - \gamma I_t - \mu I_t \tag{F.3}$$

$$R_{t+1} - R_t = \gamma I_t \tag{F.4}$$

$$D_{t+1} - D_t = \mu I_t \tag{F.5}$$

To simplify Eq. (F.3), I make a simplifying assumption—that $S_t \approx N$. This assumption is especially reasonable in the earlier periods of disease spread. For a sense of how reasonable this assumption is, I consider two edge cases with the largest difference between S and N. First, Italy had 5,883 confirmed cases by the 1st week of March (Section 3), and with a population of approximately 60 million, translates to $S/N \approx 0.999902$. A second example from 2021 is India, where an approximate snapshot of 30,500,000 cases, 400,000 deaths, and 30,000,000 recovered from a population of 1,390,000,000 translates to $S/N \approx 0.96$. Italy and India are two of the regions most severely hit in the early periods. Most other regions would have paths where $S_t \approx N$. Hence, setting $S_t/N = 1$ simplifies Eq. (F.3) to Eq. (F.6).

$$I_{t+1} - I_t = (\beta_t - \gamma - \mu)\, I_t \tag{F.6}$$

$$C_t = I_t + R_t + D_t \tag{F.7}$$

Eq. (F.7) defines the cumulative number of cases at any point in time t, which, together with Eqs. (F.4) to (F.6), implies that the dynamics of cases over time is defined by Eq. (F.8).

$$C_{t+1} - C_t = \left(I_{t+1} - I_t\right) + (R_{t+1} - R_t) + (D_{t+1} - D_t) = \beta_t I_t \tag{F.8}$$

If trafficking increases the contact rate proportionally, this implies that the contact rate β_t is really:

$$\beta_t = \tilde{\beta}_t(1 + \tau T), \tag{F.9}$$

where T is the relative trafficking inflow risk (relative TIP inflow) measure so that Eq. (F.8) becomes

$$C_{t+1} - C_t = \tilde{\beta}_t(1 + \tau T) I_t.$$

Taking a log of the above equation gives:

$$\log(C_{t+1} - C_t) = \log(\tilde{\beta}_t) + \log(1 + \tau T) + \log(I_t). \tag{F.10}$$

Eq. (F.10) can then be estimated under a regression framework where i indexes country,

$$\log(C_{i,t+1} - C_{it}) = \pi_0 + \tau T_i + \pi_1 \log(\hat{I}_{it}) + \xi_{it}, \tag{F.11}$$

with the non-augmented contact rate $\tilde{\beta}$ subsumed inside the constant π_0 (or the time fixed-effects when treated as time-varying). $\tau > 0$ facilitates the testable hypothesis of whether trafficking increases the increases in cumulative cases through increasing contact rate. Given Eq. (F.9), τT also captures the proportional increase in the contact rate arising from the trafficking inflow risk (T).

Eq. (F.10) implies a unitary elasticity, where a 1% increase in the number of infections (I) leads to a 1% increase in the growth of cases per capita ($C_{i,t+1} - C_{it}$). $\pi_1 = 1$, therefore, facilitates a test of whether Eq. (F.11) correctly reflects SIRD dynamics (at least without additional modification of T or $\hat{I}$).

I_{it} is unobserved and is estimated using $\hat{I}_{it}$, which is generated from

$$\begin{aligned} \hat{I}_{it} &= (\tilde{R}_0\tilde{\gamma})\hat{I}_{i,t-1} - \tilde{\gamma}\hat{I}_{i,t-1} - \tilde{\mu}\hat{I}_{i,t-1} + \hat{I}_{i,t-1} \\ &= \left[1 + (\tilde{R}_0\tilde{\gamma}) - \tilde{\gamma} - \tilde{\mu}\right]\hat{I}_{i,t-1}, \end{aligned} \tag{F.12}$$

where $\tilde{R}_0\tilde{\gamma}$ replaces the contact rate β.

To operationalize $\hat{I}$, I set $\hat{I}_{it^*}$ to be equal to the first recorded C_{it} for country i that is greater than the cutoff of 3, as defined in Eq. (F.13). The cutoff is not simply the first non-zero record to avoid setting $\hat{I}_{it^*}$ to a small value that affects the dynamic path. Setting the cutoff to 1 only results in numerical differences.

The three components remaining for $\hat{I}_{it^*}$ are the SIRD parameters: γ, R_0, and μ, for the recovery rate, reproduction number, and mortality rate. In the estimations, I generate $\hat{I}_{it}$ according to a combination of parameters assumptions: $\tilde{\gamma} \in \left\{\frac{1}{12}, \frac{1}{8}, \frac{1}{6}, \frac{1}{4}\right\}$, $\tilde{R}_0 \in \{3, 3.5, 4\}$, and $\tilde{\mu}$ is always set to 0.01, giving twelve different sets of $\hat{I}$.

$$\hat{I}_{it} = \begin{cases} C_{it^*} \text{ from } \operatorname{Arg\,min}_t\{C_{it}\} \text{ s.t. } C_{it} > 3, \text{ if } t = t^* \\ \left[1 + (\tilde{R}_0\tilde{\gamma}) - \tilde{\gamma} - \tilde{\mu}\right]\hat{I}_{i,t-1}, \text{ if } t > t^* \\ ., \text{ if } t < t^* \end{cases} \tag{F.13}$$

Appendix G. SIRD: Tabulation of Results

All estimates in this section are from COVID-19 numbers at the country-week level (Hale et al., 2021). The outcome variable is (i) the log change in the stock of confirmed cases as defined in Eq. (4) or (ii) the fatality rate (deaths per thousand cases) as the placebo outcome. All models have the trafficking risk measure (Relative TIP inflow) as the dependent variable, and the log stock of the infected population under the SIRD modeling, with the corresponding post-estimation test to confirm that its coefficient equals one (Section 7).

Each table considers twelve vectors of simulated infection by assuming different values of the reproduction number R_0 and recovery rate γ (Section 7). The risk of true mortality rate μ is always set to 0.01. All models include the 13 region dummies as region-by-week of year fixed effects, country fixed effects, week fixed effects, and the stringency index and economic support index as government COVID-19 response (Hale et al., 2021).

SIRD-based results: Cases, OLS

Table G1
Relative TIP Inflow as Contact Rate in SIRD Model
(Cases, Jan–Mar 2020, OLS)

	(1)	(2)	(3)	(4)	(5)	(6)	(7)	(8)	(9)	(10)	(11)	(12)
	Dependent variable is $\log(C_{it} - C_{i,t-1})$											
	$R_0 = 3$				$R_0 = 3.5$				$R_0 = 4$			
	$\gamma = \frac{1}{12}$	$\gamma = \frac{1}{8}$	$\gamma = \frac{1}{6}$	$\gamma = \frac{1}{4}$	$\gamma = \frac{1}{12}$	$\gamma = \frac{1}{8}$	$\gamma = \frac{1}{6}$	$\gamma = \frac{1}{4}$	$\gamma = \frac{1}{12}$	$\gamma = \frac{1}{8}$	$\gamma = \frac{1}{6}$	$\gamma = \frac{1}{4}$
Relative TIP inflow	0.19**	0.16**	0.14*	0.10	0.17**	0.14*	0.12	0.08	0.16**	0.13*	0.10	0.07
	(0.08)	(0.08)	(0.08)	(0.07)	(0.08)	(0.08)	(0.07)	(0.07)	(0.08)	(0.07)	(0.07)	(0.07)
$\log(I_{it})$	0.91***	1.04***	1.12***	1.16***	0.98***	1.10***	1.15***	1.13***	1.04***	1.14***	1.16***	1.08***
	(0.17)	(0.15)	(0.14)	(0.12)	(0.16)	(0.15)	(0.13)	(0.11)	(0.15)	(0.14)	(0.12)	(0.10)
p-val, $\log(I_{it}) = 1$	0.61	0.79	0.41	0.20	0.92	0.48	0.25	0.25	0.79	0.31	0.20	0.45
Stringency index	Yes	Yes	Yes	Yes	Yes	Yes	Yes	Yes	Yes	Yes	Yes	Yes
Econ. Support index	Yes	Yes	Yes	Yes	Yes	Yes	Yes	Yes	Yes	Yes	Yes	Yes
Week fixed effects	Yes	Yes	Yes	Yes	Yes	Yes	Yes	Yes	Yes	Yes	Yes	Yes
Region-by-WoY fixed effects	Yes	Yes	Yes	Yes	Yes	Yes	Yes	Yes	Yes	Yes	Yes	Yes
R^2	0.67	0.70	0.72	0.76	0.68	0.72	0.74	0.78	0.70	0.73	0.76	0.79
Countries	146	146	146	146	146	146	146	146	146	146	146	146
Weeks	10	10	10	10	10	10	10	10	10	10	10	10
Obs.	532	532	532	532	532	532	532	532	532	532	532	532

Notes—Table reports estimates of the relative risk of TIP inflow and the log of the stock of infected population under the SIRD modeling from Eq. (4). The dependent variable is the log change in the stock of confirmed cases. Each of the twelve columns uses a particular simulation of the stock of infected population by assuming values of the reproduction number R_0 and recovery rate γ. The risk of true mortality rate μ is always set to 0.01. All regressions include the 13 region dummies as region-by-week of-year fixed effects. The stringency index and economic support index as government COVID-19 response comes from the OxCGRT repository (Oxford COVID-19 Government Response Tracker, Hale et al. 2021). *** $p < 0.01$, ** $p < 0.05$, * $p < 0.1$.

Table G2
Relative TIP Inflow as Contact Rate in SIRD Model
(Cases, Apr–Dec 2020, OLS)

	(1)	(2)	(3)	(4)	(5)	(6)	(7)	(8)	(9)	(10)	(11)	(12)
	Dependent variable is $\log(C_{it} - C_{i,t-1})$											
	$R_0 = 3$				$R_0 = 3.5$				$R_0 = 4$			
	$\gamma = \frac{1}{12}$	$\gamma = \frac{1}{8}$	$\gamma = \frac{1}{6}$	$\gamma = \frac{1}{4}$	$\gamma = \frac{1}{12}$	$\gamma = \frac{1}{8}$	$\gamma = \frac{1}{6}$	$\gamma = \frac{1}{4}$	$\gamma = \frac{1}{12}$	$\gamma = \frac{1}{8}$	$\gamma = \frac{1}{6}$	$\gamma = \frac{1}{4}$
Relative TIP inflow	–0.08	–0.09	–0.10	–0.12	–0.09	–0.10	–0.11	–0.12	–0.09	–0.11	–0.12	–0.12
	(0.08)	(0.08)	(0.08)	(0.08)	(0.08)	(0.08)	(0.08)	(0.08)	(0.08)	(0.08)	(0.08)	(0.08)
$\log(I_{it})$	0.69***	0.75***	0.76***	0.69***	0.73***	0.76***	0.73***	0.63***	0.75***	0.75***	0.69***	0.58***
	(0.15)	(0.13)	(0.12)	(0.12)	(0.14)	(0.13)	(0.12)	(0.11)	(0.13)	(0.12)	(0.12)	(0.11)
p-val, $\log(I_{it}) = 1$	0.05	0.07	0.05	0.01	0.06	0.06	0.03	0.00	0.07	0.04	0.01	0.00
Stringency index	Yes	Yes	Yes	Yes	Yes	Yes	Yes	Yes	Yes	Yes	Yes	Yes
Econ. Support index	Yes	Yes	Yes	Yes	Yes	Yes	Yes	Yes	Yes	Yes	Yes	Yes
Week fixed effects	Yes	Yes	Yes	Yes	Yes	Yes	Yes	Yes	Yes	Yes	Yes	Yes
Region-by-WoY fixed effects	Yes	Yes	Yes	Yes	Yes	Yes	Yes	Yes	Yes	Yes	Yes	Yes
R^2	0.57	0.58	0.59	0.61	0.58	0.59	0.60	0.61	0.58	0.60	0.61	0.61
Countries	161	161	161	161	161	161	161	161	161	161	161	161
Weeks	39	39	39	39	39	39	39	39	39	39	39	39
Obs.	6,217	6,217	6,217	6,217	6,217	6,217	6,217	6,217	6,217	6,217	6,217	6,217

Notes—Table reports estimates of the relative risk of TIP inflow and the log of the stock of infected population under the SIRD modeling from Eq. (4). The dependent variable is the log change in the stock of confirmed cases. Each of the twelve columns uses a particular simulation of the stock of infected population by assuming values of the reproduction number R_0 and recovery rate γ. The risk of true mortality rate μ is always set to 0.01. All regressions include the 13 region dummies as region-by-week of-year fixed effects. The stringency index and economic support index as government COVID-19 response comes from the OxCGRT repository (Oxford COVID-19 Government Response Tracker, Hale et al. 2021). *** $p < 0.01$, ** $p < 0.05$, * $p < 0.1$.

Table G3
Relative TIP Inflow as Contact Rate in SIRD Model
(Cases, Interactions by month, OLS)

	(1)	(2)	(3)	(4)	(5)	(6)	(7)	(8)	(9)	(10)	(11)	(12)
	Dependent variable is $\log(C_{it} - C_{i,t-1})$											
	$R_0 = 3$				$R_0 = 3.5$				$R_0 = 4$			
	$\gamma = \frac{1}{12}$	$\gamma = \frac{1}{8}$	$\gamma = \frac{1}{6}$	$\gamma = \frac{1}{4}$	$\gamma = \frac{1}{12}$	$\gamma = \frac{1}{8}$	$\gamma = \frac{1}{6}$	$\gamma = \frac{1}{4}$	$\gamma = \frac{1}{12}$	$\gamma = \frac{1}{8}$	$\gamma = \frac{1}{6}$	$\gamma = \frac{1}{4}$
Jan × (Relative TIP inflow)	–0.01	–0.00	–0.00	–0.01	–0.01	–0.00	–0.01	–0.01	–0.00	–0.00	–0.01	–0.01
	(0.01)	(0.01)	(0.01)	(0.01)	(0.01)	(0.01)	(0.01)	(0.01)	(0.01)	(0.01)	(0.01)	(0.01)
Feb × (Relative TIP inflow)	0.19*	0.19*	0.18*	0.17	0.19*	0.19*	0.18	0.16	0.19*	0.18	0.17	0.15
	(0.11)	(0.11)	(0.11)	(0.11)	(0.11)	(0.11)	(0.11)	(0.11)	(0.11)	(0.11)	(0.11)	(0.11)
Mar × (Relative TIP inflow)	0.20**	0.18**	0.17**	0.15*	0.19**	0.17**	0.16**	0.15*	0.18**	0.16**	0.15*	0.14*
	(0.08)	(0.08)	(0.08)	(0.08)	(0.08)	(0.08)	(0.08)	(0.08)	(0.08)	(0.08)	(0.08)	(0.08)
Apr × (Relative TIP inflow)	0.08	0.06	0.05	0.04	0.07	0.05	0.04	0.03	0.06	0.05	0.04	0.03
	(0.10)	(0.09)	(0.09)	(0.09)	(0.09)	(0.09)	(0.09)	(0.09)	(0.09)	(0.09)	(0.09)	(0.09)
May × (Relative TIP inflow)	–0.06	–0.08	–0.09	–0.11	–0.07	–0.09	–0.10	–0.11	–0.08	–0.10	–0.11	–0.12
	(0.12)	(0.12)	(0.11)	(0.11)	(0.12)	(0.12)	(0.11)	(0.11)	(0.12)	(0.11)	(0.11)	(0.11)
Jun × (Relative TIP inflow)	–0.14	–0.15	–0.17	–0.18*	–0.14	–0.16	–0.17*	–0.19*	–0.15	–0.17*	–0.18*	–0.19**
	(0.10)	(0.10)	(0.10)	(0.10)	(0.10)	(0.10)	(0.10)	(0.10)	(0.10)	(0.10)	(0.10)	(0.10)
Jul × (Relative TIP inflow)	–0.14	–0.15*	–0.17*	–0.18**	–0.14	–0.16*	–0.18*	–0.19**	–0.15*	–0.17*	–0.18**	–0.19**
	(0.09)	(0.09)	(0.09)	(0.09)	(0.09)	(0.09)	(0.09)	(0.09)	(0.09)	(0.09)	(0.09)	(0.09)
Aug × (Relative TIP inflow)	–0.03	–0.04	–0.06	–0.07	–0.04	–0.05	–0.07	–0.08	–0.04	–0.06	–0.07	–0.09
	(0.09)	(0.09)	(0.08)	(0.08)	(0.09)	(0.08)	(0.08)	(0.08)	(0.09)	(0.08)	(0.08)	(0.08)
Sep × (Relative TIP inflow)	–0.07	–0.09	–0.10	–0.12	–0.08	–0.10	–0.11	–0.12	–0.09	–0.10	–0.12	–0.13
	(0.09)	(0.09)	(0.09)	(0.09)	(0.09)	(0.09)	(0.09)	(0.09)	(0.09)	(0.09)	(0.09)	(0.09)
Oct × (Relative TIP inflow)	–0.08	–0.09	–0.10	–0.11	–0.08	–0.10	–0.11	–0.12	–0.09	–0.10	–0.11	–0.12
	(0.09)	(0.09)	(0.09)	(0.09)	(0.09)	(0.09)	(0.09)	(0.09)	(0.09)	(0.09)	(0.09)	(0.09)
Nov × (Relative TIP inflow)	–0.11	–0.12	–0.12	–0.13	–0.12	–0.12	–0.13	–0.13	–0.12	–0.12	–0.13	–0.14
	(0.09)	(0.09)	(0.09)	(0.09)	(0.09)	(0.09)	(0.09)	(0.09)	(0.09)	(0.09)	(0.09)	(0.09)
Dec × (Relative TIP inflow)	–0.16*	–0.16*	–0.17*	–0.18**	–0.16*	–0.17*	–0.17*	–0.18**	–0.16*	–0.17*	–0.18**	–0.18**
	(0.09)	(0.09)	(0.09)	(0.09)	(0.09)	(0.09)	(0.09)	(0.09)	(0.09)	(0.09)	(0.09)	(0.09)
$\text{Log}(I_{it})$	0.70***	0.77***	0.77***	0.71***	0.74***	0.78***	0.75***	0.65***	0.77***	0.76***	0.71***	0.60***
	(0.15)	(0.13)	(0.12)	(0.12)	(0.14)	(0.12)	(0.12)	(0.11)	(0.13)	(0.12)	(0.12)	(0.11)
p-val, $\text{Log}(I_{it}) = 1$	0.05	0.08	0.07	0.01	0.07	0.07	0.04	0.00	0.08	0.05	0.01	0.00
Stringency index	Yes	Yes	Yes	Yes	Yes	Yes	Yes	Yes	Yes	Yes	Yes	Yes
Econ. Support index	Yes	Yes	Yes	Yes	Yes	Yes	Yes	Yes	Yes	Yes	Yes	Yes
Week fixed effects	Yes	Yes	Yes	Yes	Yes	Yes	Yes	Yes	Yes	Yes	Yes	Yes
Region-by-WoY fixed effects	Yes	Yes	Yes	Yes	Yes	Yes	Yes	Yes	Yes	Yes	Yes	Yes
R^2	0.59	0.60	0.61	0.63	0.60	0.61	0.62	0.63	0.60	0.62	0.63	0.63
Countries	161	161	161	161	161	161	161	161	161	161	161	161
Weeks	49	49	49	49	49	49	49	49	49	49	49	49
Obs.	6,749	6,749	6,749	6,749	6,749	6,749	6,749	6,749	6,749	6,749	6,749	6,749

Notes—Table reports estimates of the relative risk of TIP inflow and the log of the stock of infected population under the SIRD modeling from Eq. (4), for the months Jan–Dec 2020. The dependent variable is the log change in the stock of confirmed cases. The relative TIP inflow measure partially interacts with the month dummies so that the coefficients are absolute effects. Each of the twelve columns uses a particular simulation of the stock of infected population by assuming values of the reproduction number R_0 and recovery rate γ. The risk of true mortality rate μ is always set to 0.01. All regressions include the 13 region dummies as region-by-week of-year fixed effects. The stringency index and economic support index as government COVID-19 response comes from the OxCGRT repository (Hale et al. 2021). *** $p < 0.01$, ** $p < 0.05$, * $p < 0.1$.

SIRD-based falsification results: CFR, OLS

Table G4
Relative TIP Inflow as Contact Rate in SIRD Model
(CFR, Jan–Mar 2020, OLS)

	(1)	(2)	(3)	(4)	(5)	(6)	(7)	(8)	(9)	(10)	(11)	(12)
	Dependent variable is Case Fatality Rate (CFR)											
	$R_0 = 3$				$R_0 = 3.5$				$R_0 = 4$			
	$\gamma = \frac{1}{12}$	$\gamma = \frac{1}{8}$	$\gamma = \frac{1}{6}$	$\gamma = \frac{1}{4}$	$\gamma = \frac{1}{12}$	$\gamma = \frac{1}{8}$	$\gamma = \frac{1}{6}$	$\gamma = \frac{1}{4}$	$\gamma = \frac{1}{12}$	$\gamma = \frac{1}{8}$	$\gamma = \frac{1}{6}$	$\gamma = \frac{1}{4}$
Relative TIP inflow	0.27	0.27	0.28	0.31	0.27	0.27	0.29	0.33	0.27	0.28	0.31	0.35
	(1.65)	(1.68)	(1.71)	(1.76)	(1.67)	(1.71)	(1.74)	(1.78)	(1.68)	(1.73)	(1.76)	(1.79)
$\text{Log}(I_{it})$	0.99	0.74	0.50	0.11	0.86	0.56	0.29	–0.09	0.74	0.39	0.11	–0.22
	(4.34)	(4.41)	(4.36)	(4.04)	(4.39)	(4.39)	(4.23)	(3.72)	(4.41)	(4.30)	(4.04)	(3.40)
p-val, $\text{Log}(I_{it}) = 1$	1.00	0.95	0.91	0.83	0.98	0.92	0.87	0.77	0.95	0.89	0.83	0.72
Stringency index	Yes	Yes	Yes	Yes	Yes	Yes	Yes	Yes	Yes	Yes	Yes	Yes
Econ. Support index	Yes	Yes	Yes	Yes	Yes	Yes	Yes	Yes	Yes	Yes	Yes	Yes
Week fixed effects	Yes	Yes	Yes	Yes	Yes	Yes	Yes	Yes	Yes	Yes	Yes	Yes
Region-by-WoY fixed effects	Yes	Yes	Yes	Yes	Yes	Yes	Yes	Yes	Yes	Yes	Yes	Yes
R^2	0.17	0.16	0.16	0.16	0.17	0.16	0.16	0.16	0.16	0.16	0.16	0.16
Countries	146	146	146	146	146	146	146	146	146	146	146	146
Weeks	10	10	10	10	10	10	10	10	10	10	10	10
Obs.	533	533	533	533	533	533	533	533	533	533	533	533

Notes—Table reports estimates of the relative risk of TIP inflow and the log of the stock of infected population under the SIRD modeling from Eq. (4). The dependent variable is the case fatality rate (COVID-19 deaths divided by COVID-19 confirmed cases). Each of the twelve columns uses a particular simulation of the stock of infected population by assuming values of the reproduction number R_0 and recovery rate γ. The risk of true mortality rate μ is always set to 0.01. All regressions include the 13 region dummies as region-by-week of-year fixed effects. The stringency index and economic support index as government COVID-19 response comes from the OxCGRT repository (Oxford COVID-19 Government Response Tracker, Hale et al. 2021). *** $p < 0.01$, ** $p < 0.05$, * $p < 0.1$.

Table G5

Relative TIP Inflow as Contact Rate in SIRD Model
(CFR, Apr–Dec 2020, OLS)

	(1)	(2)	(3)	(4)	(5)	(6)	(7)	(8)	(9)	(10)	(11)	(12)
	Dependent variable is Case Fatality Rate (CFR)											
	$R_0 = 3$				$R_0 = 3.5$				$R_0 = 4$			
	$\gamma = \frac{1}{12}$	$\gamma = \frac{1}{8}$	$\gamma = \frac{1}{6}$	$\gamma = \frac{1}{4}$	$\gamma = \frac{1}{12}$	$\gamma = \frac{1}{8}$	$\gamma = \frac{1}{6}$	$\gamma = \frac{1}{4}$	$\gamma = \frac{1}{12}$	$\gamma = \frac{1}{8}$	$\gamma = \frac{1}{6}$	$\gamma = \frac{1}{4}$
Relative TIP inflow	0.60	0.61	0.62	0.65	0.60	0.62	0.63	0.66	0.61	0.63	0.65	0.67
	(1.38)	(1.35)	(1.32)	(1.28)	(1.36)	(1.33)	(1.30)	(1.27)	(1.35)	(1.31)	(1.28)	(1.26)
$\text{Log}(I_{it})$	0.36	–0.01	–0.27	–0.52	0.16	–0.21	–0.43	–0.60	–0.01	–0.36	–0.52	–0.62
	(3.20)	(3.31)	(3.29)	(3.03)	(3.28)	(3.30)	(3.17)	(2.79)	(3.31)	(3.24)	(3.03)	(2.57)
p-val, $\text{Log}(I_{it}) = 1$	0.84	0.76	0.70	0.61	0.80	0.71	0.65	0.57	0.76	0.68	0.61	0.53
Stringency index	Yes	Yes	Yes	Yes	Yes	Yes	Yes	Yes	Yes	Yes	Yes	Yes
Econ. Support index	Yes	Yes	Yes	Yes	Yes	Yes	Yes	Yes	Yes	Yes	Yes	Yes
Week fixed effects	Yes	Yes	Yes	Yes	Yes	Yes	Yes	Yes	Yes	Yes	Yes	Yes
Region-by-WoY fixed effects	Yes	Yes	Yes	Yes	Yes	Yes	Yes	Yes	Yes	Yes	Yes	Yes
R^2	0.19	0.19	0.19	0.19	0.19	0.19	0.19	0.19	0.19	0.19	0.19	0.19
Countries	161	161	161	161	161	161	161	161	161	161	161	161
Weeks	39	39	39	39	39	39	39	39	39	39	39	39
Obs.	6,224	6,224	6,224	6,224	6,224	6,224	6,224	6,224	6,224	6,224	6,224	6,224

Notes—Table reports estimates of the relative risk of TIP inflow and the log of the stock of infected population under the SIRD modeling from Eq. (4). The dependent variable is the case fatality rate (COVID-19 deaths divided by COVID-19 confirmed cases). Each of the twelve columns uses a particular simulation of the stock of infected population by assuming values of the reproduction number R_0 and recovery rate γ. The risk of true mortality rate μ is always set to 0.01. All regressions include the 13 region dummies as region-by-week of-year fixed effects. The stringency index and economic support index as government COVID-19 response comes from the OxCGRT repository (Oxford COVID-19 Government Response Tracker, Hale et al. 2021). *** p < 0.01, ** p < 0.05, * p < 0.1.

Table G6

Relative TIP Inflow as Contact Rate in SIRD Model
(CFR, Interactions by month, OLS)

	(1)	(2)	(3)	(4)	(5)	(6)	(7)	(8)	(9)	(10)	(11)	(12)
	Dependent variable is Case Fatality Rate (CFR)											
	$R_0 = 3$				$R_0 = 3.5$				$R_0 = 4$			
	$\gamma = \frac{1}{12}$	$\gamma = \frac{1}{8}$	$\gamma = \frac{1}{6}$	$\gamma = \frac{1}{4}$	$\gamma = \frac{1}{12}$	$\gamma = \frac{1}{8}$	$\gamma = \frac{1}{6}$	$\gamma = \frac{1}{4}$	$\gamma = \frac{1}{12}$	$\gamma = \frac{1}{8}$	$\gamma = \frac{1}{6}$	$\gamma = \frac{1}{4}$
Jan × (Relative TIP inflow)	0.01	–0.01	–0.02	–0.03	0.00	–0.02	–0.03	–0.04	–0.01	–0.03	–0.03	–0.04
	(0.17)	(0.18)	(0.18)	(0.16)	(0.18)	(0.18)	(0.17)	(0.15)	(0.18)	(0.17)	(0.16)	(0.14)
Feb × (Relative TIP inflow)	–2.82	–2.85	–2.87	–2.88	–2.84	–2.86	–2.87	–2.87	–2.85	–2.87	–2.88	–2.87
	(3.51)	(3.53)	(3.54)	(3.55)	(3.52)	(3.54)	(3.54)	(3.55)	(3.53)	(3.54)	(3.55)	(3.55)
Mar × (Relative TIP inflow)	0.56	0.59	0.61	0.66	0.57	0.61	0.64	0.68	0.59	0.63	0.66	0.69
	(1.56)	(1.57)	(1.58)	(1.60)	(1.57)	(1.58)	(1.59)	(1.61)	(1.57)	(1.59)	(1.60)	(1.62)
Apr × (Relative TIP inflow)	3.76**	3.78**	3.80**	3.83**	3.77**	3.79**	3.82**	3.85**	3.78**	3.81**	3.83**	3.86**
	(1.84)	(1.84)	(1.85)	(1.85)	(1.84)	(1.84)	(1.85)	(1.86)	(1.84)	(1.85)	(1.85)	(1.86)
May × (Relative TIP inflow)	3.51**	3.53**	3.55**	3.59**	3.52**	3.54**	3.57**	3.61**	3.53**	3.56**	3.59**	3.62**
	(1.71)	(1.68)	(1.67)	(1.65)	(1.69)	(1.67)	(1.66)	(1.64)	(1.68)	(1.66)	(1.65)	(1.64)
Jun × (Relative TIP inflow)	2.94	2.96	2.98*	3.02*	2.95	2.98*	3.00*	3.04*	2.96	2.99*	3.02*	3.05*
	(1.83)	(1.79)	(1.77)	(1.73)	(1.81)	(1.77)	(1.75)	(1.72)	(1.79)	(1.76)	(1.73)	(1.71)
Jul × (Relative TIP inflow)	1.80	1.81	1.83	1.87	1.81	1.83	1.85	1.89	1.81	1.84	1.87	1.90
	(1.77)	(1.73)	(1.70)	(1.66)	(1.75)	(1.71)	(1.68)	(1.64)	(1.73)	(1.69)	(1.66)	(1.63)
Aug × (Relative TIP inflow)	0.15	0.16	0.18	0.21	0.16	0.18	0.20	0.23	0.16	0.19	0.21	0.25
	(1.63)	(1.60)	(1.56)	(1.52)	(1.62)	(1.57)	(1.54)	(1.50)	(1.60)	(1.55)	(1.52)	(1.48)
Sep × (Relative TIP inflow)	–0.44	–0.43	–0.42	–0.38	–0.44	–0.42	–0.40	–0.37	–0.43	–0.41	–0.38	–0.35
	(1.42)	(1.39)	(1.35)	(1.30)	(1.41)	(1.36)	(1.32)	(1.28)	(1.39)	(1.34)	(1.30)	(1.26)
Oct × (Relative TIP inflow)	–1.35	–1.35	–1.33	–1.31	–1.35	–1.34	–1.32	–1.29	–1.35	–1.33	–1.31	–1.28
	(1.40)	(1.37)	(1.34)	(1.29)	(1.39)	(1.34)	(1.31)	(1.26)	(1.37)	(1.32)	(1.29)	(1.25)
Nov × (Relative TIP inflow)	–2.21*	–2.21*	–2.21*	–2.20*	–2.21*	–2.21*	–2.20*	–2.19*	–2.21*	–2.21*	–2.20*	–2.19*
	(1.31)	(1.29)	(1.28)	(1.26)	(1.30)	(1.28)	(1.27)	(1.25)	(1.29)	(1.28)	(1.26)	(1.24)
Dec × (Relative TIP inflow)	–2.23*	–2.23*	–2.23*	–2.21*	–2.23*	–2.23*	–2.22*	–2.21*	–2.23*	–2.22*	–2.21*	–2.20*
	(1.27)	(1.25)	(1.24)	(1.21)	(1.26)	(1.24)	(1.22)	(1.20)	(1.25)	(1.23)	(1.21)	(1.19)
$\text{Log}(I_{it})$	0.25	–0.13	–0.38	–0.63	0.04	–0.33	–0.54	–0.70	–0.13	–0.47	–0.63	–0.71
	(3.16)	(3.26)	(3.22)	(2.96)	(3.23)	(3.24)	(3.11)	(2.73)	(3.26)	(3.17)	(2.96)	(2.51)
p-val, $\text{Log}(I_{it}) = 1$	0.81	0.73	0.67	0.58	0.77	0.68	0.62	0.53	0.73	0.64	0.58	0.50
Stringency index	Yes	Yes	Yes	Yes	Yes	Yes	Yes	Yes	Yes	Yes	Yes	Yes
Econ. Support index	Yes	Yes	Yes	Yes	Yes	Yes	Yes	Yes	Yes	Yes	Yes	Yes
Week fixed effects	Yes	Yes	Yes	Yes	Yes	Yes	Yes	Yes	Yes	Yes	Yes	Yes
Region-by-WoY fixed effects	Yes	Yes	Yes	Yes	Yes	Yes	Yes	Yes	Yes	Yes	Yes	Yes
R^2	0.21	0.21	0.21	0.21	0.21	0.21	0.21	0.21	0.21	0.21	0.21	0.21
Countries	161	161	161	161	161	161	161	161	161	161	161	161
Weeks	49	49	49	49	49	49	49	49	49	49	49	49
Obs.	6,757	6,757	6,757	6,757	6,757	6,757	6,757	6,757	6,757	6,757	6,757	6,757

Notes—Table reports estimates of the relative risk of TIP inflow and the log of the stock of infected population under the SIRD modeling from Eq. (4), for the months Jan–Dec 2020. The dependent variable is the case fatality rate (COVID-19 deaths divided by COVID-19 confirmed cases). The relative TIP inflow measure partially interacts with the month dummies so that the coefficients are absolute effects. Each of the twelve columns uses a particular simulation of the stock of infected population by assuming values of the reproduction number R_0 and recovery rate γ. The risk of true mortality rate μ is always set to 0.01. All regressions include the 13 region dummies as region-by-week of-year fixed effects. The stringency index and economic support index as government COVID-19 response comes from the OxCGRT repository (Hale et al. 2021). *** p < 0.01, ** p < 0.05, * p < 0.1.

SIRD-based results: Cases, 2SLS

Table G7

Relative TIP Inflow as Contact Rate in SIRD Model
(Cases, Jan–Mar 2020, 2SLS)

	(1)	(2)	(3)	(4)	(5)	(6)	(7)	(8)	(9)	(10)	(11)	(12)
	Dependent variable is $\log(C_{it} - C_{i,t-1})$											
	$R_0 = 3$				$R_0 = 3.5$				$R_0 = 4$			
	$\gamma = \frac{1}{12}$	$\gamma = \frac{1}{8}$	$\gamma = \frac{1}{6}$	$\gamma = \frac{1}{4}$	$\gamma = \frac{1}{12}$	$\gamma = \frac{1}{8}$	$\gamma = \frac{1}{6}$	$\gamma = \frac{1}{4}$	$\gamma = \frac{1}{12}$	$\gamma = \frac{1}{8}$	$\gamma = \frac{1}{6}$	$\gamma = \frac{1}{4}$
Relative TIP inflow	–0.05	–0.06	–0.07	–0.08	–0.06	–0.07	–0.08	–0.09	–0.06	–0.07	–0.08	–0.10
	(0.21)	(0.21)	(0.20)	(0.19)	(0.21)	(0.20)	(0.19)	(0.18)	(0.21)	(0.20)	(0.19)	(0.17)
$\text{Log}(I_{it})$	0.98***	1.12***	1.20***	1.24***	1.06***	1.19***	1.24***	1.21***	1.12***	1.23***	1.24***	1.15***
	(0.17)	(0.16)	(0.15)	(0.14)	(0.16)	(0.15)	(0.15)	(0.13)	(0.16)	(0.15)	(0.14)	(0.13)
p-val, $\text{Log}(I_{it}) = 1$	0.89	0.46	0.19	0.09	0.73	0.23	0.10	0.12	0.46	0.13	0.09	0.22
First-stage F-stat	13.85	13.9	14	14.29	13.86	13.97	14.14	14.52	13.9	14.07	14.29	14.72
Stringency index	Yes	Yes	Yes	Yes	Yes	Yes	Yes	Yes	Yes	Yes	Yes	Yes
Econ. Support index	Yes	Yes	Yes	Yes	Yes	Yes	Yes	Yes	Yes	Yes	Yes	Yes
Week fixed effects	Yes	Yes	Yes	Yes	Yes	Yes	Yes	Yes	Yes	Yes	Yes	Yes
Region-by-WoY fixed effects	Yes	Yes	Yes	Yes	Yes	Yes	Yes	Yes	Yes	Yes	Yes	Yes
Countries	145	145	145	145	145	145	145	145	145	145	145	145
Weeks	10	10	10	10	10	10	10	10	10	10	10	10
Obs.	530	530	530	530	530	530	530	530	530	530	530	530

Notes—Table reports estimates of the relative risk of TIP inflow and the log of the stock of infected population under the SIRD modeling from Eq. (4). The dependent variable is the log change in the stock of confirmed cases. Each of the twelve columns uses a particular simulation of the stock of infected population by assuming values of the reproduction number R_0 and recovery rate γ. The risk of true mortality rate μ is always set to 0.01. All regressions include the 13 region dummies as region-by-week of-year fixed effects. The stringency index and economic support index as government COVID-19 response comes from the OxCGRT repository (Oxford COVID-19 Government Response Tracker, Hale et al. 2021). *** $p < 0.01$, ** $p < 0.05$, * $p < 0.1$.

Table G8

Relative TIP Inflow as Contact Rate in SIRD Model
(Cases, Apr–Dec 2020, 2SLS)

	(1)	(2)	(3)	(4)	(5)	(6)	(7)	(8)	(9)	(10)	(11)	(12)
	Dependent variable is $\log(C_{it} - C_{i,t-1})$											
	$R_0 = 3$				$R_0 = 3.5$				$R_0 = 4$			
	$\gamma = \frac{1}{12}$	$\gamma = \frac{1}{8}$	$\gamma = \frac{1}{6}$	$\gamma = \frac{1}{4}$	$\gamma = \frac{1}{12}$	$\gamma = \frac{1}{8}$	$\gamma = \frac{1}{6}$	$\gamma = \frac{1}{4}$	$\gamma = \frac{1}{12}$	$\gamma = \frac{1}{8}$	$\gamma = \frac{1}{6}$	$\gamma = \frac{1}{4}$
Relative TIP inflow	–0.54	–0.54	–0.53	–0.53*	–0.54	–0.53	–0.53*	–0.53*	–0.54	–0.53*	–0.53*	–0.53*
	(0.33)	(0.33)	(0.32)	(0.32)	(0.33)	(0.33)	(0.32)	(0.32)	(0.33)	(0.32)	(0.32)	(0.31)
$\text{Log}(I_{it})$	0.74***	0.81***	0.82***	0.76***	0.78***	0.82***	0.80***	0.69***	0.81***	0.81***	0.76***	0.64***
	(0.16)	(0.15)	(0.15)	(0.15)	(0.15)	(0.15)	(0.15)	(0.14)	(0.15)	(0.15)	(0.15)	(0.14)
p-val, $\text{Log}(I_{it}) = 1$	0.11	0.21	0.22	0.10	0.16	0.23	0.16	0.03	0.21	0.20	0.10	0.01
First-stage F-stat	13.16	13.26	13.35	13.5	13.2	13.33	13.43	13.57	13.26	13.39	13.5	13.62
Stringency index	Yes	Yes	Yes	Yes	Yes	Yes	Yes	Yes	Yes	Yes	Yes	Yes
Econ. Support index	Yes	Yes	Yes	Yes	Yes	Yes	Yes	Yes	Yes	Yes	Yes	Yes
Week fixed effects	Yes	Yes	Yes	Yes	Yes	Yes	Yes	Yes	Yes	Yes	Yes	Yes
Region-by-WoY fixed effects	Yes	Yes	Yes	Yes	Yes	Yes	Yes	Yes	Yes	Yes	Yes	Yes
Countries	160	160	160	160	160	160	160	160	160	160	160	160
Weeks	39	39	39	39	39	39	39	39	39	39	39	39
Obs.	6,178	6,178	6,178	6,178	6,178	6,178	6,178	6,178	6,178	6,178	6,178	6,178

Notes—Table reports estimates of the relative risk of TIP inflow and the log of the stock of infected population under the SIRD modeling from Eq. (4). The dependent variable is the log change in the stock of confirmed cases. Each of the twelve columns uses a particular simulation of the stock of infected population by assuming values of the reproduction number R_0 and recovery rate γ. The risk of true mortality rate μ is always set to 0.01. All regressions include the 13 region dummies as region-by-week of-year fixed effects. The stringency index and economic support index as government COVID-19 response comes from the OxCGRT repository (Oxford COVID-19 Government Response Tracker, Hale et al. 2021). *** $p < 0.01$, ** $p < 0.05$, * $p < 0.1$.

Table G9

Relative TIP Inflow as Contact Rate in SIRD Model
(Cases, Interactions by month, 2SLS)

	(1)	(2)	(3)	(4)	(5)	(6)	(7)	(8)	(9)	(10)	(11)	(12)
	Dependent variable is $\log(C_{it} - C_{i,t-1})$											
	$R_0 = 3$				$R_0 = 3.5$				$R_0 = 4$			
	$\gamma = \frac{1}{12}$	$\gamma = \frac{1}{8}$	$\gamma = \frac{1}{6}$	$\gamma = \frac{1}{4}$	$\gamma = \frac{1}{12}$	$\gamma = \frac{1}{8}$	$\gamma = \frac{1}{6}$	$\gamma = \frac{1}{4}$	$\gamma = \frac{1}{12}$	$\gamma = \frac{1}{8}$	$\gamma = \frac{1}{6}$	$\gamma = \frac{1}{4}$
Jan × (Relative TIP inflow)	–0.00	–0.00	–0.00	–0.00	–0.00	0.00	–0.00	–0.01	–0.00	–0.00	–0.00	–0.01
	(0.01)	(0.01)	(0.01)	(0.01)	(0.01)	(0.01)	(0.01)	(0.01)	(0.01)	(0.01)	(0.01)	(0.02)
Feb × (Relative TIP inflow)	0.42***	0.42***	0.42***	0.41***	0.42***	0.42***	0.41***	0.40***	0.42***	0.41***	0.41***	0.39***
	(0.10)	(0.10)	(0.10)	(0.10)	(0.10)	(0.10)	(0.10)	(0.10)	(0.10)	(0.10)	(0.10)	(0.10)
Mar × (Relative TIP inflow)	–0.14	–0.15	–0.15	–0.16	–0.14	–0.15	–0.16	–0.16	–0.15	–0.16	–0.16	–0.16
	(0.23)	(0.22)	(0.21)	(0.20)	(0.23)	(0.22)	(0.21)	(0.20)	(0.22)	(0.21)	(0.20)	(0.19)
Apr × (Relative TIP inflow)	–0.32	–0.34	–0.35	–0.37	–0.33	–0.35	–0.36	–0.38	–0.34	–0.36	–0.37	–0.38
	(0.39)	(0.39)	(0.38)	(0.37)	(0.39)	(0.38)	(0.37)	(0.36)	(0.39)	(0.37)	(0.37)	(0.36)
May × (Relative TIP inflow)	–0.60	–0.62	–0.62	–0.63	–0.61	–0.62	–0.63	–0.63	–0.62	–0.63	–0.63	–0.63
	(0.48)	(0.48)	(0.47)	(0.46)	(0.48)	(0.47)	(0.46)	(0.45)	(0.48)	(0.47)	(0.46)	(0.45)
Jun × (Relative TIP inflow)	–0.74	–0.76	–0.77*	–0.78*	–0.75	–0.77*	–0.78*	–0.79*	–0.76	–0.77*	–0.78*	–0.79*
	(0.47)	(0.46)	(0.46)	(0.45)	(0.46)	(0.46)	(0.45)	(0.45)	(0.46)	(0.46)	(0.45)	(0.44)
Jul × (Relative TIP inflow)	–0.81*	–0.82**	–0.83**	–0.85**	–0.82*	–0.83**	–0.84**	–0.85**	–0.82**	–0.84**	–0.85**	–0.85**
	(0.41)	(0.41)	(0.41)	(0.41)	(0.41)	(0.41)	(0.41)	(0.40)	(0.41)	(0.41)	(0.41)	(0.40)
Aug × (Relative TIP inflow)	–0.36	–0.37	–0.38	–0.40	–0.37	–0.38	–0.39	–0.40	–0.37	–0.39	–0.40	–0.41
	(0.35)	(0.35)	(0.34)	(0.34)	(0.35)	(0.34)	(0.34)	(0.34)	(0.35)	(0.34)	(0.34)	(0.34)
Sep × (Relative TIP inflow)	–0.43	–0.44	–0.45	–0.46	–0.44	–0.45	–0.46	–0.47	–0.44	–0.45	–0.46	–0.47
	(0.34)	(0.34)	(0.33)	(0.33)	(0.34)	(0.33)	(0.33)	(0.33)	(0.34)	(0.33)	(0.33)	(0.33)
Oct × (Relative TIP inflow)	–0.46	–0.46	–0.45	–0.45	–0.46	–0.45	–0.45	–0.45	–0.46	–0.45	–0.45	–0.45
	(0.31)	(0.31)	(0.31)	(0.30)	(0.31)	(0.31)	(0.30)	(0.30)	(0.31)	(0.30)	(0.30)	(0.30)
Nov × (Relative TIP inflow)	–0.53*	–0.49*	–0.46	–0.41	–0.51*	–0.46	–0.43	–0.39	–0.49*	–0.44	–0.41	–0.38
	(0.29)	(0.29)	(0.30)	(0.31)	(0.29)	(0.29)	(0.30)	(0.31)	(0.29)	(0.30)	(0.31)	(0.32)
Dec × (Relative TIP inflow)	–0.61**	–0.57*	–0.54*	–0.50	–0.59*	–0.55*	–0.51*	–0.48	–0.57*	–0.53*	–0.50	–0.47
	(0.30)	(0.30)	(0.30)	(0.31)	(0.30)	(0.30)	(0.31)	(0.31)	(0.30)	(0.31)	(0.31)	(0.32)
$\text{Log}(I_{it})$	0.76***	0.83***	0.85***	0.79***	0.81***	0.85***	0.82***	0.72***	0.83***	0.84***	0.79***	0.66***
	(0.16)	(0.15)	(0.14)	(0.14)	(0.15)	(0.14)	(0.14)	(0.14)	(0.15)	(0.14)	(0.14)	(0.13)
p-val, $\text{Log}(I_{it}) = 1$	0.13	0.27	0.29	0.14	0.21	0.29	0.22	0.05	0.27	0.26	0.14	0.01
Stringency index	Yes	Yes	Yes	Yes	Yes	Yes	Yes	Yes	Yes	Yes	Yes	Yes
Econ. Support index	Yes	Yes	Yes	Yes	Yes	Yes	Yes	Yes	Yes	Yes	Yes	Yes
Week fixed effects	Yes	Yes	Yes	Yes	Yes	Yes	Yes	Yes	Yes	Yes	Yes	Yes
Region-by-WoY fixed effects	Yes	Yes	Yes	Yes	Yes	Yes	Yes	Yes	Yes	Yes	Yes	Yes
Countries	160	160	160	160	160	160	160	160	160	160	160	160
Weeks	49	49	49	49	49	49	49	49	49	49	49	49
Obs.	6,708	6,708	6,708	6,708	6,708	6,708	6,708	6,708	6,708	6,708	6,708	6,708

Notes—Table reports estimates of the relative risk of TIP inflow and the log of the stock of infected population under the SIRD modeling from Eq. (4), for the months Jan–Dec 2020. The dependent variable is the log change in the stock of confirmed cases. The relative TIP inflow measure partially interacts with the month dummies so that the coefficients are absolute effects. Each of the twelve columns uses a particular simulation of the stock of infected population by assuming values of the reproduction number R_0 and recovery rate γ. The risk of true mortality rate μ is always set to 0.01. All regressions include the 13 region dummies as region-by-week of-year fixed effects. The stringency index and economic support index as government COVID-19 response comes from the OxCGRT repository (Hale et al. 2021). *** p < 0.01, ** p < 0.05, * p < 0.1.

SIRD-based falsification results: CFR, 2SLS

Table G10

Relative TIP Inflow as Contact Rate in SIRD Model
(CFR, Jan–Mar 2020, 2SLS)

	(1)	(2)	(3)	(4)	(5)	(6)	(7)	(8)	(9)	(10)	(11)	(12)
	Dependent variable is Case Fatality Rate (CFR)											
	$R_0 = 3$				$R_0 = 3.5$				$R_0 = 4$			
	$\gamma = \frac{1}{12}$	$\gamma = \frac{1}{8}$	$\gamma = \frac{1}{6}$	$\gamma = \frac{1}{4}$	$\gamma = \frac{1}{12}$	$\gamma = \frac{1}{8}$	$\gamma = \frac{1}{6}$	$\gamma = \frac{1}{4}$	$\gamma = \frac{1}{12}$	$\gamma = \frac{1}{8}$	$\gamma = \frac{1}{6}$	$\gamma = \frac{1}{4}$
Relative TIP inflow	–3.95	–3.96	–3.98	–3.99	–3.96	–3.97	–3.99	–4.00	–3.96	–3.98	–3.99	–4.01
	(2.61)	(2.61)	(2.61)	(2.61)	(2.61)	(2.61)	(2.61)	(2.62)	(2.61)	(2.61)	(2.61)	(2.62)
$\text{Log}(I_{it})$	1.92	2.01	2.03	1.92	1.98	2.03	1.99	1.78	2.01	2.02	1.92	1.63
	(4.36)	(4.38)	(4.29)	(3.94)	(4.38)	(4.32)	(4.13)	(3.63)	(4.38)	(4.22)	(3.94)	(3.33)
p-val, $\text{Log}(I_{it}) = 1$	0.83	0.82	0.81	0.82	0.82	0.81	0.81	0.83	0.82	0.81	0.82	0.85
First-stage F-stat	13.85	13.9	14.01	14.3	13.87	13.98	14.15	14.52	13.9	14.08	14.3	14.72
Stringency index	Yes	Yes	Yes	Yes	Yes	Yes	Yes	Yes	Yes	Yes	Yes	Yes
Econ. Support index	Yes	Yes	Yes	Yes	Yes	Yes	Yes	Yes	Yes	Yes	Yes	Yes
Week fixed effects	Yes	Yes	Yes	Yes	Yes	Yes	Yes	Yes	Yes	Yes	Yes	Yes
Region-by-WoY fixed effects	Yes	Yes	Yes	Yes	Yes	Yes	Yes	Yes	Yes	Yes	Yes	Yes
Countries	145	145	145	145	145	145	145	145	145	145	145	145
Weeks	10	10	10	10	10	10	10	10	10	10	10	10
Obs.	531	531	531	531	531	531	531	531	531	531	531	531

Notes—Table reports estimates of the relative risk of TIP inflow and the log of the stock of infected population under the SIRD modeling from Eq. (4). The dependent variable is the case fatality rate (COVID-19 deaths divided by COVID-19 confirmed cases). Each of the twelve columns uses a particular simulation of the stock of infected population by assuming values of the reproduction number R_0 and recovery rate γ. The risk of true mortality rate μ is always set to 0.01. All regressions include the 13 region dummies as region-by-week of-year fixed effects. The stringency index and economic support index as government COVID-19 response comes from the OxCGRT repository (Oxford COVID-19 Government Response Tracker, Hale et al. 2021). *** p < 0.01, ** p < 0.05, * p < 0.1.

Table G11

Relative TIP Inflow as Contact Rate in SIRD Model (CFR, Apr–Dec 2020, 2SLS)

	(1)	(2)	(3)	(4)	(5)	(6)	(7)	(8)	(9)	(10)	(11)	(12)
	Dependent variable is Case Fatality Rate (CFR)											
	$R_0 = 3$				$R_0 = 3.5$				$R_0 = 4$			
	$\gamma = \frac{1}{12}$	$\gamma = \frac{1}{8}$	$\gamma = \frac{1}{6}$	$\gamma = \frac{1}{4}$	$\gamma = \frac{1}{12}$	$\gamma = \frac{1}{8}$	$\gamma = \frac{1}{6}$	$\gamma = \frac{1}{4}$	$\gamma = \frac{1}{12}$	$\gamma = \frac{1}{8}$	$\gamma = \frac{1}{6}$	$\gamma = \frac{1}{4}$
Relative TIP inflow	–5.77	–5.77	–5.77	–5.77	–5.77	–5.77	–5.77	–5.76	–5.77	–5.77	–5.77	–5.76
	(3.88)	(3.88)	(3.88)	(3.88)	(3.88)	(3.88)	(3.88)	(3.88)	(3.88)	(3.88)	(3.88)	(3.88)
$\text{Log}(I_{it})$	0.79	0.68	0.57	0.40	0.74	0.59	0.47	0.31	0.68	0.52	0.40	0.25
	(3.49)	(3.46)	(3.33)	(2.97)	(3.49)	(3.37)	(3.16)	(2.71)	(3.46)	(3.25)	(2.97)	(2.48)
p-val, $\text{Log}(I_{it}) = 1$	0.95	0.93	0.90	0.84	0.94	0.90	0.87	0.80	0.93	0.88	0.84	0.76
First-stage F-stat	13.09	13.19	13.28	13.43	13.14	13.26	13.36	13.5	13.19	13.33	13.43	13.55
Stringency index	Yes	Yes	Yes	Yes	Yes	Yes	Yes	Yes	Yes	Yes	Yes	Yes
Econ. Support index	Yes	Yes	Yes	Yes	Yes	Yes	Yes	Yes	Yes	Yes	Yes	Yes
Week fixed effects	Yes	Yes	Yes	Yes	Yes	Yes	Yes	Yes	Yes	Yes	Yes	Yes
Region-by-WoY fixed effects	Yes	Yes	Yes	Yes	Yes	Yes	Yes	Yes	Yes	Yes	Yes	Yes
Countries	160	160	160	160	160	160	160	160	160	160	160	160
Weeks	39	39	39	39	39	39	39	39	39	39	39	39
Obs.	6,185	6,185	6,185	6,185	6,185	6,185	6,185	6,185	6,185	6,185	6,185	6,185

Notes—Table reports estimates of the relative risk of TIP inflow and the log of the stock of infected population under the SIRD modeling from Eq. (4). The dependent variable is the case fatality rate (COVID-19 deaths divided by COVID-19 confirmed cases). Each of the twelve columns uses a particular simulation of the stock of infected population by assuming values of the reproduction number R_0 and recovery rate γ. The risk of true mortality rate μ is always set to 0.01. All regressions include the 13 region dummies as region-by-week of-year fixed effects. The stringency index and economic support index as government COVID-19 response comes from the OxCGRT repository (Oxford COVID-19 Government Response Tracker, Hale et al. 2021). *** p < 0.01, ** p < 0.05, * p < 0.1.

Table G12

Relative TIP Inflow as Contact Rate in SIRD Model (CFR, Interactions by month, 2SLS)

	(1)	(2)	(3)	(4)	(5)	(6)	(7)	(8)	(9)	(10)	(11)	(12)
	Dependent variable is Case Fatality Rate (CFR)											
	$R_0 = 3$				$R_0 = 3.5$				$R_0 = 4$			
	$\gamma = \frac{1}{12}$	$\gamma = \frac{1}{8}$	$\gamma = \frac{1}{6}$	$\gamma = \frac{1}{4}$	$\gamma = \frac{1}{12}$	$\gamma = \frac{1}{8}$	$\gamma = \frac{1}{6}$	$\gamma = \frac{1}{4}$	$\gamma = \frac{1}{12}$	$\gamma = \frac{1}{8}$	$\gamma = \frac{1}{6}$	$\gamma = \frac{1}{4}$
Jan × (Relative TIP inflow)	0.04	0.04	0.03	0.02	0.04	0.03	0.03	0.02	0.04	0.03	0.02	0.01
	(0.18)	(0.17)	(0.17)	(0.15)	(0.18)	(0.17)	(0.16)	(0.13)	(0.17)	(0.16)	(0.15)	(0.12)
Feb × (Relative TIP inflow)	–3.44	–3.45	–3.46	–3.48	–3.45	–3.46	–3.47	–3.49	–3.45	–3.47	–3.48	–3.49
	(3.18)	(3.17)	(3.16)	(3.15)	(3.17)	(3.16)	(3.15)	(3.15)	(3.17)	(3.15)	(3.15)	(3.15)
Mar × (Relative TIP inflow)	–4.09	–4.09	–4.09	–4.09	–4.09	–4.09	–4.09	–4.09	–4.09	–4.09	–4.09	–4.08
	(2.90)	(2.90)	(2.91)	(2.92)	(2.90)	(2.91)	(2.91)	(2.92)	(2.90)	(2.91)	(2.92)	(2.92)
Apr × (Relative TIP inflow)	–6.76	–6.77	–6.77	–6.76	–6.77	–6.77	–6.76	–6.75	–6.77	–6.77	–6.76	–6.75
	(5.45)	(5.46)	(5.48)	(5.50)	(5.46)	(5.47)	(5.49)	(5.51)	(5.46)	(5.48)	(5.50)	(5.51)
May × (Relative TIP inflow)	–5.38	–5.38	–5.37	–5.36	–5.38	–5.37	–5.37	–5.35	–5.38	–5.37	–5.36	–5.35
	(5.32)	(5.33)	(5.33)	(5.34)	(5.32)	(5.33)	(5.34)	(5.35)	(5.33)	(5.34)	(5.34)	(5.35)
Jun × (Relative TIP inflow)	–4.29	–4.29	–4.29	–4.28	–4.29	–4.29	–4.28	–4.27	–4.29	–4.29	–4.28	–4.27
	(5.22)	(5.22)	(5.22)	(5.22)	(5.22)	(5.22)	(5.22)	(5.22)	(5.22)	(5.22)	(5.22)	(5.22)
Jul × (Relative TIP inflow)	–6.37	–6.37	–6.37	–6.37	–6.37	–6.37	–6.37	–6.36	–6.37	–6.37	–6.37	–6.36
	(5.56)	(5.55)	(5.54)	(5.54)	(5.56)	(5.55)	(5.54)	(5.54)	(5.55)	(5.54)	(5.54)	(5.54)
Aug × (Relative TIP inflow)	–6.77	–6.78	–6.78	–6.78	–6.77	–6.78	–6.78	–6.78	–6.78	–6.78	–6.78	–6.78
	(4.69)	(4.68)	(4.67)	(4.65)	(4.68)	(4.67)	(4.66)	(4.65)	(4.68)	(4.66)	(4.65)	(4.65)
Sep × (Relative TIP inflow)	–5.33	–5.34	–5.35	–5.36	–5.34	–5.35	–5.35	–5.36	–5.34	–5.35	–5.36	–5.36
	(3.79)	(3.78)	(3.77)	(3.75)	(3.78)	(3.77)	(3.76)	(3.75)	(3.78)	(3.76)	(3.75)	(3.75)
Oct × (Relative TIP inflow)	–5.01	–5.01	–5.01	–5.01	–5.01	–5.01	–5.01	–5.02	–5.01	–5.01	–5.01	–5.02
	(3.15)	(3.15)	(3.15)	(3.16)	(3.15)	(3.15)	(3.16)	(3.16)	(3.15)	(3.16)	(3.16)	(3.16)
Nov × (Relative TIP inflow)	–6.18*	–6.16*	–6.15*	–6.14*	–6.17*	–6.15*	–6.14*	–6.14*	–6.16*	–6.14*	–6.14*	–6.15*
	(3.27)	(3.34)	(3.40)	(3.50)	(3.30)	(3.39)	(3.46)	(3.55)	(3.34)	(3.43)	(3.50)	(3.58)
Dec × (Relative TIP inflow)	–5.84*	–5.82*	–5.81*	–5.80*	–5.83*	–5.81*	–5.80*	–5.81*	–5.82*	–5.80*	–5.80*	–5.81*
	(3.00)	(3.06)	(3.11)	(3.19)	(3.03)	(3.10)	(3.15)	(3.23)	(3.06)	(3.13)	(3.19)	(3.26)
$\text{Log}(I_{it})$	0.86	0.75	0.64	0.46	0.81	0.66	0.54	0.36	0.75	0.59	0.46	0.30
	(3.49)	(3.45)	(3.33)	(2.98)	(3.48)	(3.37)	(3.16)	(2.72)	(3.45)	(3.25)	(2.98)	(2.49)
p-val, $\text{Log}(I_{it}) = 1$	0.97	0.94	0.91	0.86	0.96	0.92	0.88	0.82	0.94	0.90	0.86	0.78
Stringency index	Yes	Yes	Yes	Yes	Yes	Yes	Yes	Yes	Yes	Yes	Yes	Yes
Econ. Support index	Yes	Yes	Yes	Yes	Yes	Yes	Yes	Yes	Yes	Yes	Yes	Yes
Week fixed effects	Yes	Yes	Yes	Yes	Yes	Yes	Yes	Yes	Yes	Yes	Yes	Yes
Region-by-WoY fixed effects	Yes	Yes	Yes	Yes	Yes	Yes	Yes	Yes	Yes	Yes	Yes	Yes
Countries	160	160	160	160	160	160	160	160	160	160	160	160
Weeks	49	49	49	49	49	49	49	49	49	49	49	49
Obs.	6,716	6,716	6,716	6,716	6,716	6,716	6,716	6,716	6,716	6,716	6,716	6,716

Notes—Table reports estimates of the relative risk of TIP inflow and the log of the stock of infected population under the SIRD modeling from Eq. (4), for the months Jan–Dec 2020. The dependent variable is the case fatality rate (COVID-19 deaths divided by COVID-19 confirmed cases). The relative TIP inflow measure partially interacts with the month dummies so that the coefficients are absolute effects. Each of the twelve columns uses a particular simulation of the stock of infected population by assuming values of the reproduction number R_0 and recovery rate γ. The risk of true mortality rate μ is always set to 0.01. All regressions include the 13 region dummies as region-by-week of-year fixed effects. The stringency index and economic support index as government COVID-19 response comes from the OxCGRT repository (Hale et al. 2021). *** p < 0.01, ** p < 0.05, * p < 0.1.